

2006

Distinction between deterministic and random beam fanning in photorefractive materials

Arun M. Venkataraman
University of Dayton

Follow this and additional works at: https://ecommons.udayton.edu/graduate_theses

Recommended Citation

Venkataraman, Arun M., "Distinction between deterministic and random beam fanning in photorefractive materials" (2006). *Graduate Theses and Dissertations*. 6127.
https://ecommons.udayton.edu/graduate_theses/6127

This Thesis is brought to you for free and open access by the Theses and Dissertations at eCommons. It has been accepted for inclusion in Graduate Theses and Dissertations by an authorized administrator of eCommons. For more information, please contact mschlangen1@udayton.edu, ecommons@udayton.edu.

**DISTINCTION BETWEEN DETERMINISTIC AND RANDOM
BEAM FANNING IN PHOTOREFRACTIVE MATERIALS**

Thesis

Submitted to
School of Engineering
UNIVERSITY OF DAYTON

In partial fulfillment of the requirement for the degree of
Master of Science in Electro-Optics

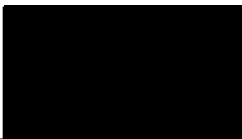
By
Arun M Venkataraman

School of Engineering
UNIVERSITY OF DAYTON

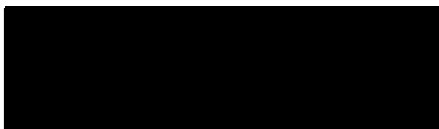
Dayton, Ohio
August 2006

**DISTINCTION BETWEEN DETERMINISTIC AND RANDOM BEAM
FANNING IN PHOTOREFRACTIVE MATERIAL**


APPROVED BY:




Partha P. Banerjee, Ph.D.
Advisory Committee Chairman
Professor, Department of Electrical
Engineering




Joseph W. Haus, Ph.D.
Committee Member
Professor, Electro-Optics
Program



Andrew M. Sarangan, Ph.D.
Committee Member
Associate Professor, Electro-Optics
Program



Donald L. Moon, Ph.D.
Associate Dean
Graduate Engineering Programs & Research,
School of Engineering



Joseph E. Saliba, Ph.D., P.E.
Dean, School of Engineering

ABSTRACT

DISTINCTION BETWEEN DETERMINISTIC AND RANDOM BEAM FANNING IN PHOTOREFRACTIVE MATERIALS

Name: Arun M. Venkataraman

University of Dayton, August 2006

Advisor: Partha P. Banerjee

Photorefractive beam fanning is observed in diffusion dominated materials such as barium titanate and photovoltaic materials such as lithium niobate. Beam fanning in barium titanate has been extensively used to generate self-pumped phase conjugation. Beam fanning patterns in lithium niobate have been utilized in characterization of the photorefractive material. Two types of beam fanning have been shown to exist: deterministic beam fanning which results from the shape of the beam, and random beam fanning which originates from scattering of the incident beam from the surface and bulk of the crystal. In this paper, we report on a careful analysis of both kinds of fanning, using a focused Gaussian beam of varying waists and incorporating randomness in amplitude and phase at the surface and through the bulk of the photorefractive material. We show that in photorefractive barium titanate, deterministic beam fanning, characterized by a deflection of the main lobe of the beam in the far field and an additional sideband, may dominate over waist sizes in the tens of microns, whereas random beam fanning, characterized by multiple lobes, dominate over waist sizes larger

than tens of microns. Further we extend this analysis to simulate phase conjugation in PR media, where we conclude from our simulation results that the phase conjugation via backscattering cannot be substantiated from the back reflection of the crystal.

ACKNOWLEDGEMENTS

I dedicate this work to my parents and my dear sister. They are my source of inspiration and it is their unconditional love makes this life meaningful.

I sincerely thank my advisor Dr. Partha P. Banerjee for his patient and meticulous advising. I want to thank my committee members Dr. Joseph W. Haus and Dr. Andrew Saranagan for their time and support.

Finally, I am also grateful to all my friends Nagamani Pathrui, Sangameshwar Sonth, Sudeepthi Nellutla, Swathi Gayam, Yoga L. Srinivas Kantamani and many others for their never ending support and timely help.

TABLE OF CONTENTS

ABSTRACT	iii
ACKNOWLEDGEMENT	v
LIST OF FIGURES	viii
LIST OF TABLE	xi
LIST OF SYMBOLS	xiii
I. INTRODUCTION TO PHOTOREFRACTIVE EFFECT.....	1
1.1 Background and Motivation.....	1
1.2 Introduction to Photorefractive Effect.....	2
1.3 Basic Phenomena: The Band Transport Model	3
1.4 Kukhtarev Equations	4
1.5 Index Grating Formation in Photorefractive Media.....	6
1.6 Two Wave Mixing	9
1.7 Application of Photorefractive	11
II. SIMULATION OF BEAM PROPAGATION IN NONLINEAR MEDIA.....	13
2.1 Introduction	13
2.2 Motivation	13
2.3. Beam Propagation Method: Theory and Algorithm.....	14
2.3.1 Theory	14
2.3.2 Algorithm	18

2.3 Simulation of Beam Propagation in Nonlinear Kerr Media.....	19
2.4 Simulation Results.....	20
2.6 Conclusion.....	26
III. DISTINCTION BETWEEN DETERMINISTIC AND RANDOM BEAM FANNING IN PHOTOREFRACTIVE MATERIALS.....	27
3.1 Introduction	27
3.2 Induced Refractive Index Change in Photorefractive Media	28
3.3. Simulation of DBF	30
3.4. Incorporation of RBF	36
3.5 Effect of Beam Waist on Beam Fanning.....	38
3.6 Effect of Randomness on Beam Fanning.....	41
3.7 Effect of Length of Sample in Beam Fanning.....	44
3.8 Summary	46
IV. SIMULATION OF PHASE CONJUGATION IN PHOTOREFRACTIVE MEDIA AND CONCLUSION	48
4.1 Introduction	48
4.2 Simulation of Phase Conjugation in Photorefractive via Backscattering	48
4.3 Simulation of Mutually Pumped Phase conjugation in Photorefractive due to Two- wave Mixing.....	52
4.4 Summary, Conclusions and Future Work	54
APPENDIX	56
REFERENCES.....	66

LIST OF FIGURES

Figure 1.1	Band transport model of PR effect.....	3
Figure 1.2	PR effect.....	8
Figure 1.3	Two wave mixing in PR media. (a) Codirectional two-wave mixing and (b) Contradirectional two-wave mixing.....	11
Figure 2.1	Qualitative understanding for the angular spectrum for the angular spectrum.....	15
Figure 2.2	Beam propagation in homogeneous medium with index n	16
Figure 2.3	Schematic diagram of beam propagation method.....	17
Figure 2.4	Flow chart for BPM.....	18
Figure 2.5a	Almost linear propagation in nonlinear medium ($z_{\max} = 30 z_r$).....	20
Figure 2.5b	Almost linear propagation in nonlinear medium at various instants.....	21
Figure 2.6a	Self focusing in nonlinear Kerr media.....	22
Figure 2.6b	Self focusing profiles in nonlinear Kerr media at various distances.....	22
Figure 2.7	Periodic self focusing of Gaussian beam.....	23
Figure 2.8a	Second order soliton propagation.....	24
Figure 2.8b	Second order soliton profiles at various distances.....	25
Figure 2.9a	Third order soliton propagation.....	25
Figure 2.9b	Third order soliton profiles at various distances.....	26

Figure 3.1	Normalized intensity profile at the exit of the crystal for various beam waists.....	31
Figure 3.2	Normalized intensity profile at far field for various beam waists.....	32
Figure 3.3	Normalized intensity profile at far field of thick sample for various power levels (Beam Width = 8 μm and sample length = 1 cm).....	33
Figure 3.4	Normalized intensity profile at far field of thin sample for various power level (Beam Width = 40 μm and sample length = 1 cm).....	34
Figure 3.5	Normalized intensity profile at far field for various X-cut crystals (Beam Width = 8 μm and sample length = 1 cm).....	35
Figure 3.6a	Normalized beam profile at far field for BaTiO_3 crystal.....	37
Figure 3.6b	Simulation of beam propagation in BaTiO_3 crystal giving rise to RBF...	37
Figure 3.7a	Normalized beam intensity at far field for BaTiO_3 (W = 8 microns).....	38
Figure 3.7b	Simulation of beam propagation in BaTiO_3 crystal (W = 8 microns).....	39
Figure 3.8a	Normalized beam intensity at far field for BaTiO_3 (W = 50 microns).....	39
Figure 3.8b	Simulation of beam propagation in BaTiO_3 crystal (W = 50 microns)....	40
Figure 3.9a	Normalized beam intensity at far field for BaTiO_3 (W = 80 microns).....	40
Figure 3.9b	Simulation of beam propagation in BaTiO_3 crystal (W = 80 microns)....	41
Figure 3.10a	Normalized beam intensity at far field for BaTiO_3 (W = 100 microns) with increased randomness.....	42
Figure 3.10b	Simulation of beam propagation in BaTiO_3 crystal (W = 100 microns)....	42
Figure 3.11a	Normalized beam intensity at far field for BaTiO_3 (W = 100 microns) with decreased randomness.....	43

Figure 3.11b	Simulation of beam propagation in BaTiO ₃ crystal (W = 100 microns) with decreased randomness.....	43
Figure 3.12a	Normalized beam intensity at far field for BaTiO ₃ (W = 100 microns) with sample length 0.5 cm.....	44
Figure 3.12b	Simulation of beam propagation in BaTiO ₃ crystal (W = 100 microns) with sample length 0.5 cm.....	45
Figure 3.13a	Normalized beam intensity at far field for BaTiO ₃ (W = 100 microns) with sample length 2 cm.....	45
Figure 3.13b	Simulation of Beam propagation in BaTiO ₃ crystal (W =100 microns) with sample length 2 cm.....	46
Figure 4.1a	Incident and backscattered beam for one pass.....	50
Figure 4.1b	Backscattered beam (dotted) and original beam at the initial position for one pass.....	51
Figure 4.2a	Incident and backscattered beam for 10 passes.....	51
Figure 4.2b	Backscattered beam (dotted) and original beam at the initial position for ten passes.....	52
Figure 4.3	Contrapropagating beam mixing in PR media.....	53
Figure 4.4	Backward traveling beam and original beam (dotted) at the initial position for one pass.....	54

LIST OF TABLE

Table 2.1	Beam and crystal paramaters used in simulation of beam propagation in non linear Kerr medium.....	20
Table 3.1	Distinction Between DBF and RBF.....	47

LIST OF SYMBOLS

n	Electron density
I	Intensity of the optical field
s	Cross section for the photon excitation,
\square	Rate of thermal generation of the electrons
N_A	Density of acceptors
N_D	Donor density,
N_D^+	Ionized donor density,
γ_R	Electron- ionized trap recombination rate,
J	Current density
q	Electron charge
μ	Mobility tensor
E_s	Electrostatic field
\square	Dielectric constant
ρ	Charge density
$\overline{k_1}, \overline{k_2}$	Wave vectors
\square	Grating vector period
α	Absorption coefficient
\overline{n}	Homogenous refractive index,

n_2	Kerr coefficient
w_b	Beam waist inside the medium,
I_n	Beam intensity inside the medium
L	Length of the nonlinear medium
e	Electronic charge
N_a	Acceptor concentration,
ϵ_s	Electrostatic permittivity
k_B	Boltzman constant,
T	Temperature
W	Characteristic width of the envelope of the optical field
a_x, a_y	Unit vectors
n_o	Linear ordinary refractive index
n_e	Extraordinary refractive index
r_{ij}	Linear electrooptic coefficients
θ	Angle between x axis and the c -axis of the crystal within the material

Chapter 1

Introduction to Photorefractive Effect

1.1 Background and Motivation

The photorefractive (PR) effect is a nonlinear optical effect seen in certain crystals and materials that respond to light by altering their refractive index. The effect can be used store temporary, erasable holograms and is useful for holographic data storage. PR beam fanning is a phenomenon observed in diffusion dominated materials such as barium titanate (BaTiO_3) and photovoltaic materials such as lithium niobate (LiNbO_3). Beam fanning in BaTiO_3 may result in asymmetric distortion and deflection of a single laser beam in a PR crystal also, a very small portion of the incident beam may be scattered from inhomogeneities and impurities in the crystal. The scattered components may then interact with each other and with the incident beam via two-wave mixing. This may lead to an amplification of the scattered light in the direction of the energy transfer. Beam fanning in BaTiO_3 has been extensively used to generate self-pumped phase conjugation. Beam fanning patterns in LiNbO_3 have been utilized in characterization of the PR material.

Two types of beam fanning have been shown to exist: deterministic beam fanning (DBF) which results from the shape of the beam, and random beam fanning (RBF) which originates from scattering of the incident beam from the surface and bulk of the crystal

[1-4]. Following initial work done by Banerjee and co-workers in the nineties [1,2], there has been renewed interest in beam fanning and its modeling and experimentation over the last five years [3,4]. In this thesis, we have done a careful analysis of both kinds of fanning, using a focused Gaussian beam of varying waists, powers and by incorporating randomness in amplitude and phase, both at the surface and through the bulk of the PR material. We have shown that in PR BaTiO₃, DBF, characterized by a deflection of the main lobe of the beam in the far field and an additional sideband, may dominate over waist sizes in the tens of microns, whereas RBF, characterized by multiple lobes, dominate over waist sizes larger than tens of microns. Finally we have also analyzed few phase conjugate configurations of BaTiO₃.

1.2 Introduction to Photorefractive Effect

The field of PR nonlinear optics has now been around for more than two decades. The effect first referred to as "Optical Damage" [5] was first discovered in 1966 by Ashkin et al in Bell Telephone Laboratories. They observed an optically induced variation of the index of refraction in LiNbO₃ that strongly disturbed optical beam propagation, which was affecting the critical phase matching condition for the second harmonic they were trying to generate. Some of the well know electro-optic crystal in which this effect is observed are BaTiO₃, KNbO₃, LiNbO₃, LiTaO₃, Sr_{1-x}Ba_xNb₂O₆ (SBN), Bi₁₂SiO₂₀ (BSO) [6]. It is also observed in semiconductors like InP, GaAs and also in polymers and in liquid crystals. PR-based systems have found major applications in sensing, optical computing, image processing, signal processing and many more. This

Chapter deals with the basic concepts of PR nonlinear optics. Here we discuss the band transport model through the well known Kukhtarev equations. This model also describes the formation of refractive index grating in PR crystals. This Chapter sets a stage for the future Chapters that deals with the beam fanning and phase conjugation in PR media.

1.3 Basic Phenomena: The Band Transport Model

The PR effect is a phenomenon in which the local index of refraction of a medium is changed by the illumination of a beam of light with spatial variation of the intensity [7-8]. The theory of band transport model was first published in 1977 by Kukhtarev [9] and developed in his further papers [10]. In the model, PR media are assumed to contain certain type species of impurities through doping of the material. Let us assume that all donor impurities are identical and have exactly the same energy state somewhere near the middle of the bandgap (see Fig. 1.1).

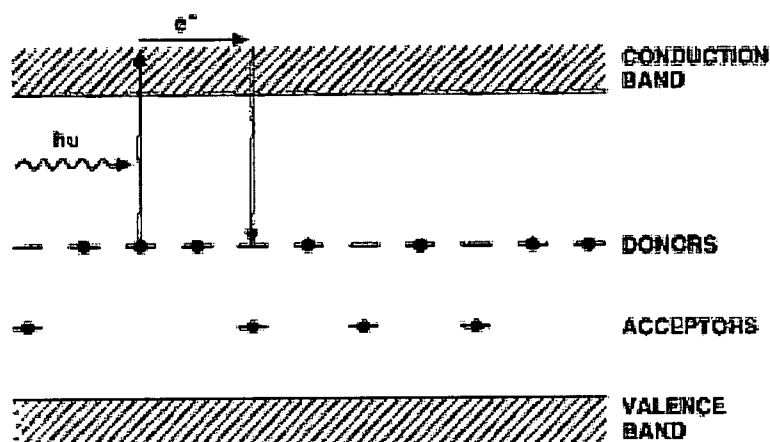


Figure 1.1 Band transport model of PR effect.

Electrons in the valence band of these donor impurities absorb photons. As the result of absorption, electrons are generated in the conduction band leaving ionized donor states behind. Due to combined drift and diffusion the ejected photoelectrons migrate into the dark regions of the crystal where they recombine with ionized donors or acceptors. This process of charge separation results in a space-charge electric field that modulates the material refractive index via the linear electro-optic effect.

As shown in Fig. 1.1 there may be residual acceptor impurities as well. Usually the density of donors is often much larger than that of the acceptor impurities. Here we assume that all acceptors are also identical. In the case when there are no electrons in the conduction band and no holes in the valence band, the density of ionized donor impurities is identical to that of the acceptor impurities. The neutral donor impurities are capable of donating electrons for photo excitation and the ionized donors are capable of capturing these photoelectrons. In the model, the acceptor impurities are incorporated in the charge balance, since they can also absorb the photoelectrons. They do not directly participate in the PR effect.

1.4 Kukhtarev Equations

Equations (1.1-1.4) written below are known as the Kukhtarev equations. These comprise the rate equations for the ionized donor density, the conservation of charge, the current density and the Gauss's law and are given by

$$\frac{\partial N_D^+}{\partial t} = (sI + \beta)(N_D - N_D^+) - \gamma_R N N_D^+, \quad (1.1)$$

$$\frac{\partial n}{\partial t} - \frac{\partial N_D^+}{\partial t} = \frac{1}{q} \nabla \cdot J, \quad (1.2)$$

$$J = qn\mu E_s + k_B T \mu \nabla n, \quad (1.3)$$

$$\nabla \cdot (\epsilon E_s) = \rho = -q(n + N_A - N_D^+), \quad (1.4)$$

where n is the total electron density, I is the intensity, s is the cross section for the photon excitation, β is the rate of thermal generation of the electrons, N_A is the density of acceptors assumed to be completely ionized from trapped photoelectrons, N_D is the donor density, N_D^+ is the ionized donor density, γ_R is the electron- ionized trap recombination rate, J is current density and q is electron charge (1.602×10^{19} C). Also, μ the mobility tensor, E_s is the electrostatic field, $k_B T$ is the product of the Boltzmann constant and temperatures, ϵ is the dielectric constant and ρ is the charge density.

For every impurity ionized, an electron is generated. On the other hand, an electron is eliminated when it is recaptured by ionized impurities. But the electrons are mobile and the impurities are stationary. This is vital mechanism for PR effect. This movement of electrons affects the electron density as shown in Eq. (1.2), the difference in generation rates for electrons and ionized donors constitutes a current density. The presence of these charge carriers (electrons) leads to a space-charge field which in turn affects the transport of the carriers. Equation (1.3) gives the current density in the medium. The current density consists of contributions from the drift of charge carriers due the electrostatic field ($qn\mu E$) and the diffusion due to the gradient of carrier density

$(k_B T \mu \nabla n)$. Note the current due photovoltaic effect is neglected in this case. Finally the electrostatic field is given by Gauss's law (Eq. (1.4)). The acceptor impurity is taken into consideration only for the charge neutrality, assuming that they are all ionized from absorbing mobile electrons.

1.5 Index Grating Formation in PR Media

Let us consider the incidence of two optical waves into a PR medium. The electric fields of the waves are given by

$$E_1 = A_1 \exp i(\omega t - \vec{k}_1 \cdot \vec{r}) \quad (1.5)$$

$$E_2 = A_2 \exp i(\omega t - \vec{k}_2 \cdot \vec{r}) \quad (1.6)$$

where A_1 and A_2 are intensity of two beams and \vec{k}_1, \vec{k}_2 are wave vectors.

The two beams will form an interference pattern with intensity

$$I = |A_1|^2 + |A_2|^2 + A_2 A_1^* \exp(-i\vec{K} \cdot \vec{r}) + A_2^* A_1 \exp(i\vec{K} \cdot \vec{r}) \quad (1.7)$$

where $\vec{K} = \vec{k}_1 - \vec{k}_2$. Note for the interference to occur, the polarization states of these two waves should not be orthogonal. For simplicity the Eq. (1.7) is written as

$$I = I_0 + \text{Re}\{I_1 \exp(-i\vec{K} \cdot \vec{r})\} \quad (1.8)$$

where I_0 and I_1 are constants and grating vector period (Λ) is related to wave vector as

$\Lambda = \frac{2\pi}{|\vec{K}|}$. In the bright regions, photo ionized charges are generated by the absorption

of photons. These charge carriers diffuse away from the bright regions leaving behind positively charged ionized donor impurities. If these charge carriers are trapped in the

dark regions, they will remain there because there is no light to re excite them. This leads to a charge separation as depicted. As a result of the illumination with periodic intensity in the PR medium, the dark regions are negatively charged and the bright regions are positively charged (see Fig. 1.2). The buildup of space charge separation will continue until the diffusion current is counterbalanced by the drift current. The space-charge density can thus be written as

$$\rho = \rho_0 \cos(\vec{K} \cdot \vec{r}), \quad (1.9)$$

where ρ_0 is a constant. Integrating the Poisson's Eq. we get

$$\vec{E} = \rho_0 \frac{\vec{K}}{K \cdot \epsilon K} \sin(\vec{K} \cdot \vec{r}). \quad (1.10)$$

From Eq. (1.9) and Eq. (1.10), it is clear that the space-charge field is shifted in space by $\pi/2$ relative to the intensity pattern. This space-charge field will induce a change in the index of refraction via the Pockels' effect. Figure 1.2 illustrates the spatial variation of the light intensity, space-charge density, space-charge field and the induced index change.

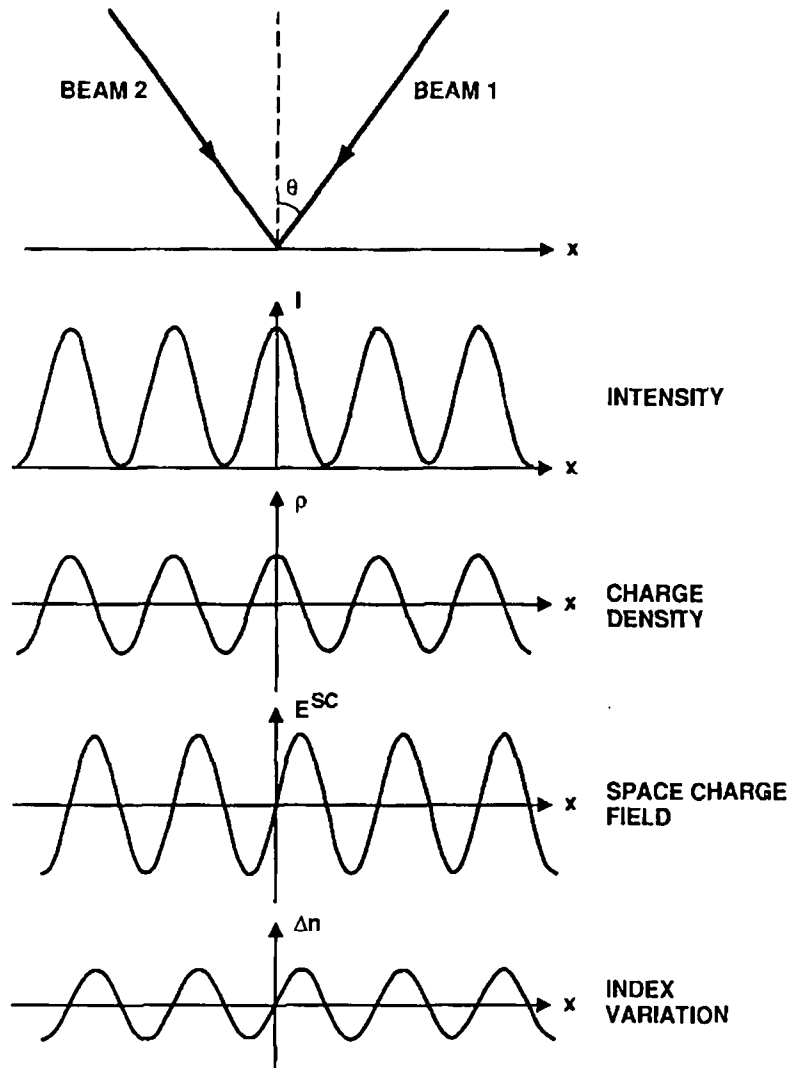


Figure 1.2 PR effect.

In summary, the PR effect consists of five fundamental processes which occur in electro-optic crystals:

- 1) photoionization of impurities and the generation of charge carriers,
- 2) Transport of these charge carriers,
- 3) Trapping of charge carriers and the formation of a space-charge density,
- 4) Formation of the photoinduced space-charge electric field, and
- 5) Formation of index grating via the linear electro-optic effect (Pockel effect).

The PR effect is a macroscopic phenomenon and requires the generation and transport of a large number of charge carriers (typically, of the order of 10^{15} cm^{-3}). The speed of grating formation is limited by the time needed to absorb a large number of photons for the particular intensity level [12]. The solution of the Kukhtarev equations have been studied and analyzed for various kind conditions and the steady-state solutions for the amplitude of the space-charge field in presented in many books [13-14].

1.6 Two-Wave Mixing

Let us consider the interaction of two laser beams inside a PR medium. If the two beams are of the same frequency, a stationary interference pattern is formed. The electric field of the two waves can be written as

$$E_j = A_j \exp(i(\omega t - k_j \cdot r)), \quad (1.11)$$

where A_1, A_2 are the wave amplitudes and ω the angular frequency. For simplicity, we assume that the medium is isotropic and both beams are polarized perpendicular to the plane of incidence. According to the model described in the last section, the intersection of these two beams induces a volume index grating via the PR effect. In general, the index grating has a spatial phase shift relative to the interference pattern. The index of refraction including the fundamental component of the intensity induced gratings can be written as

$$n = n_0 + \frac{n_1}{2} \exp(i\phi) A_1^* A_2 \exp(i\vec{K} \cdot \vec{r}) + c.c., \quad (1.12)$$

where $I = I_1 + I_2 = |A_1|^2 + |A_2|^2$ is phase, which the index grating is shifted spatially with respect to the light interference pattern and n_0 the index of refraction when no light is present. In PR media that operate by diffusion the finite spatial phase shift between the interference pattern and the induced volume index grating has been known for some time [11]. The presence of such a phase shift allows the possibility of nonreciprocal steady-state transfer energy between the beams [11].

Assume both waves propagate in the xz plane, the beams are of finite extent (i.e., comparable to the intersection of the beams), the amplitudes may depend on both I and z . Here we assume, for the sake of simplicity, that the transverse dimensions of the beams are of infinite extent so that the boundary condition requires that the wave amplitudes A_1 and A_2 be functions of z only (see Fig. 1.3). In the case of co directional coupling the Intensity solutions for both the beam are obtained using the slowly-varying amplitude approximation as [11]

$$I_1(z) = I_1(0) \frac{1 + m^{-1}}{1 + m^{-1} \exp(\gamma z)} \exp(\alpha z), \quad (1.13)$$

$$I_2(z) = I_2(0) \frac{1 + m}{1 + m \exp(\gamma z)} \exp(\alpha z), \quad (1.14)$$

where $\gamma = \frac{2\pi m_1}{\lambda \cos \phi} \sin \phi$, $m = \frac{I_1(0)}{I_2(0)}$ and α is absorption coefficient.

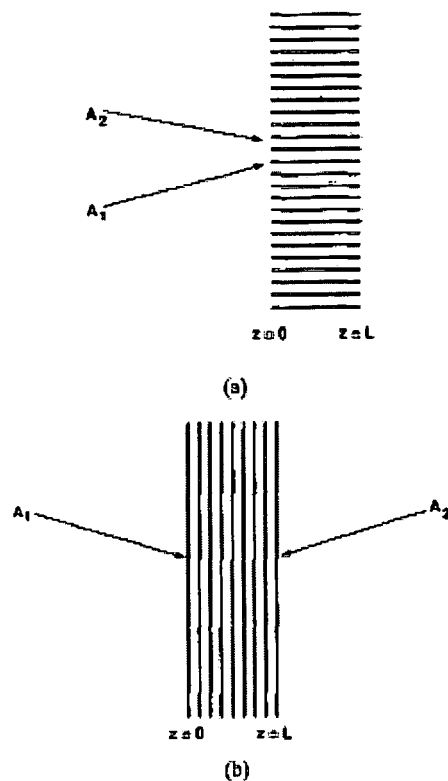


Figure 1.3 Two wave mixing in PR media. (a) Codirectional two-wave mixing and (b) contradirectional two-wave mixing [11].

1.7 Application of PR Media

No field will improve if doesn't find applications and PR nonlinear optics is no exception. The inherently parallel nature of optical information processing, coupled with its typically higher bandwidth, confers a potential advantage over conventional electronically-based processing, such as digital signal processing. PR media store real-time holograms which have memory and can provide high optical gain (20cm^{-1}) at moderately low intensities on the order of W/cm^2 , characteristics which are useful in the implementation of optical information processing architectures. PR-based systems can

be subdivided in three main categories: optical computing, image processing and signal processing. Examples of optical computing systems include associative memories and correlators [12-15], neural networks [16;], and reconfigurable array interconnects [17]. Image processing systems include functions such as image amplification [18], image thresholding [19], edge enhancement [20], amplifying spatial filtering [21], novelty filters [22]. Narrow-band filters [23] and optical heterodyning [24] are examples of signal processing systems. PR systems applications have been reviewed extensively in [4].

Chapter 2

Simulation of Beam Propagation in Nonlinear Media

2.1 Introduction

The Beam Propagation method (BPM) is well known powerful tool for analysis of beam propagation in nonuniform, anisotropic, and nonlinear media. It was developed first in underwater acoustic and seismology and then adapted to optical problems. Initially, BPM was developed for light propagation in a waveguide [27-29]. Later it was used to find how light propagates in nonlinear materials and how it changes after the propagation through the nonlinear material. A comprehensive review can be found in [30].

2.2 Motivation

BPM is a numerical simulation of the electric field and not an approximate solution to the exact wave equation [31]. In this Chapter the concept and capabilities of the beam propagation method [32], [33] are reviewed. The BPM is the most widely used propagation technique for modeling integrated and fiber-optic photonic devices, and most commercial software for such modeling is based on it. There are several reasons for the popularity of BPM. The most significant reason is that it is conceptually straightforward,

allowing rapid implementation of the basic technique. The BPM is generally a very efficient method and the computational effort is directly proportional to the number of grid points used in the numerical simulation. Another characteristic of BPM is that the approach is readily applied to complex geometries without having to develop specialized versions of the method. Furthermore, the approach automatically includes the effects of both guided and radiating fields as well as mode coupling and conversion. Finally, the BPM technique is very flexible and extensible, allowing inclusion of most effects of interest (e.g., polarization, nonlinearities) by extensions of the basic method that fit within the same overall framework. Because the simulation of the light propagation by BPM is almost always successful and for certain problems it is the only way to obtain results, thus BPM is the method of choice to simulate numerically the most complicated PR effects.

2.3. Beam Propagation Method: Theory and Algorithm

2.3.1 Theory

If the initial optical field (at a position $z = 0$) $E(x,y,0)$ is known, then the angular spectrum is obtained from the plane-wave decomposition of the field using a Fourier transform as (see Fig. 2.1)

$$A(k_x, k_y; 0) = \int_{-\infty}^{\infty} \int_{-\infty}^{\infty} E(x, y, 0) \exp[-i(k_x x + k_y y)] dx dy = F_{xy}\{E(x, y, 0)\} \quad (2.1)$$

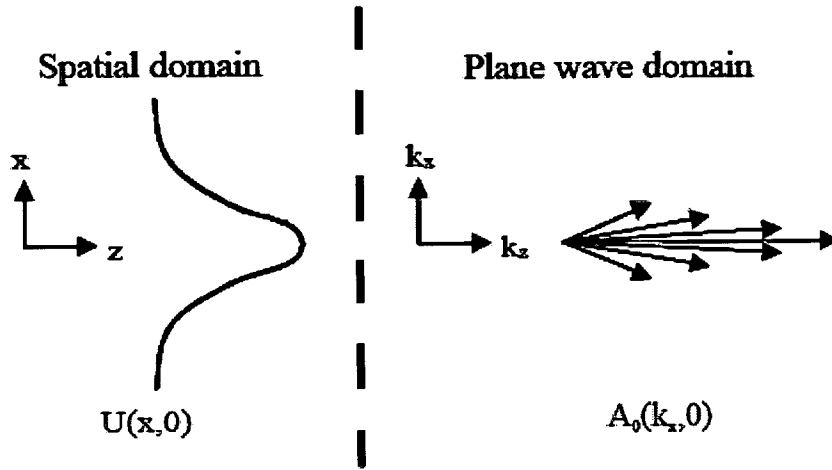


Figure 2.1 Qualitative understanding for the angular spectrum for the angular spectrum.

Then we propagate the angular spectrum through a distance Δz . The propagated angular spectrum is given by

$$A(k_x, k_y; \Delta z) = A_0(k_x, k_y, 0) \exp(i\Phi_s), \quad (2.2)$$

where Φ_s is the phase accumulated by each plane wave through Δz and given by

$$\Phi_s = \frac{\bar{n}k_0\Delta z}{\cos\theta} \approx \bar{n}k_0\Delta z \left(1 + \frac{k_x^2}{2n^2k_0^2} \right), \quad (2.3)$$

where \bar{n} is the homogenous refractive index. The above equation has been approximated for small angle (paraxial) approximation.

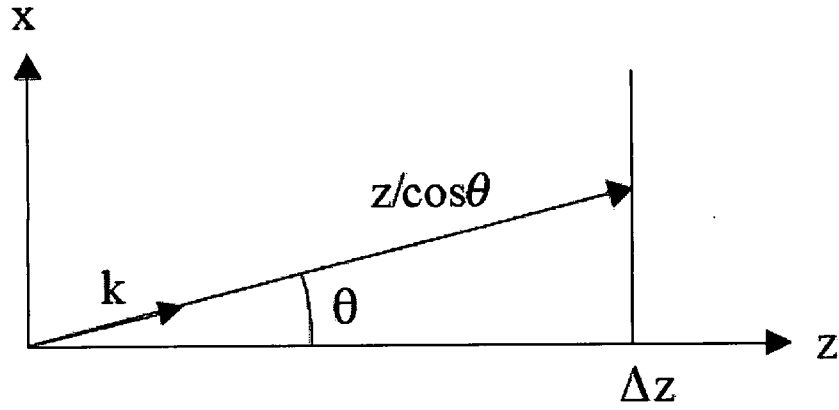


Figure 2.2 Beam propagation in homogeneous medium with index n .

The paraxial approximation in Eq. (2.3) may be used depending on the numerical aperture (NA) of the beam. The paraxial approximation is used for small NA. However, it cannot be used for high NA, because the significant amount of the decomposed plane waves may have a large angle θ . The field after the propagation by $E(x, y; \Delta z)$ is found by calculating the inverse Fourier transform of the propagated angular spectrum.

$$(E(x, y, \Delta z)) = \int_{-\infty}^{\infty} \int_{-\infty}^{\infty} A(k_x, k_y; \Delta z) \exp[i(k_x x + k_y y)] dk_x dk_y = F_{xy}^{-1}\{A(k_x, k_y; \Delta z)\}. \quad (2.4)$$

If the medium is homogeneous, the procedure of BPM stops here, since Δz can be replaced by the total propagation distance z . However, if the medium has any kind of inhomogeneity, a phase correction term is added to the field, as depicted in following equations:

$$\phi(x, y, z_0) = k_0 n(x, y, z_0) \Delta z, \quad (2.5)$$

$$\Delta \phi(x, y, z_0) = k_0 (n(x, y, z_0) - \bar{n}) \Delta z, \quad (2.6)$$

$$E(x, y, z_0 + \Delta z) = E(x, y, z_0) \exp(-i \Delta \phi(x, y, z_0)), \quad (2.7)$$

where $\phi(x, y, z_0)$ is the total phase that the plane wave propagating along the z -axis experiences and thus, the phase correction added is $\Delta\phi(x, y, z_0)$, which is the difference between Φ_s and the homogeneous phase used in the previous step. Finally, the field after propagation through Δz is found. The procedure described above is one step of the BPM for propagation through distance Δz . The steps are repeated until the desired propagation distance z is achieved (see Fig. 2.3). Thus the whole process can be written in one equation as

$$E(x, y, z + \Delta z) = F^{-1}\{F\{E(x, y, z)\} \exp(-i\Phi_s)\} \exp(i\Delta\phi\Delta z) \quad (2.8)$$

Finally the choice of Δz plays a significant role in BPM. If Δz chosen is very small then the BPM will take more time for computation; on the other hand if Δz is chosen large then the error in the BPM result will increase.

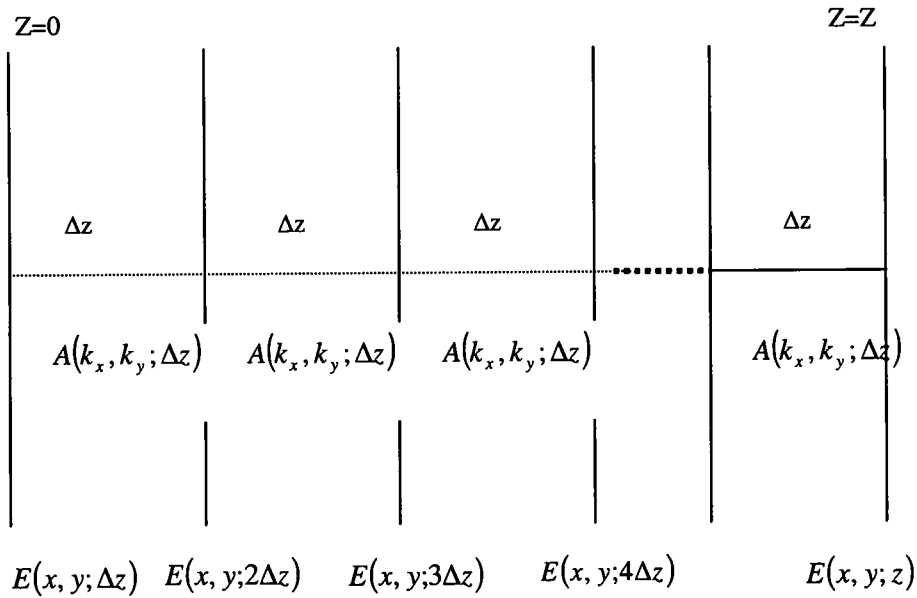


Figure 2.3 Schematic diagram of beam propagation method.

2.3.2 Algorithm

In essence BPM is diffraction and refraction done in two different steps. In the first step we obtain the plane wave spectrum (through FFT in MATLAB) and multiply it with the propagation phase. In the second step we go back to the space domain and multiply the phase correction required for the inhomogeneity or nonlinearity in the medium. These steps are repeated until we propagate the beam to desired distance. The algorithm is shown in the as of flow chart in Fig. 2.4.

$$\underbrace{E(x, y, z + \Delta z) = F^{-1}\{F\{E(x, y, z)\}\exp(-i\Phi_s)\}}_{\text{diffraction}} \underbrace{\exp(i\Delta\phi\Delta z)}_{\text{refraction}} \quad (2.9)$$

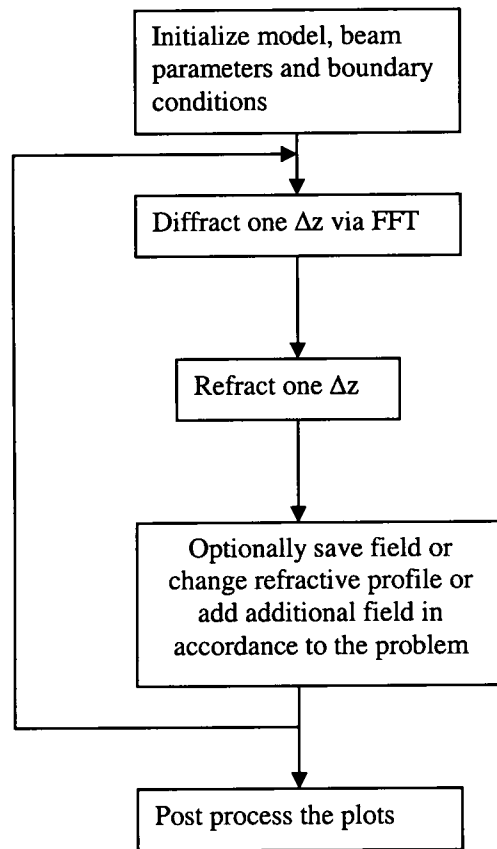


Figure 2.4 Flow chart for BPM.

2.3 Simulation of Beam Propagation in Nonlinear Kerr Media

In this Section we apply the BPM technique to simulate the angular Gaussian beam propagation in a nonlinear Kerr medium. In Kerr type of material, the index of refraction is proportional to the intensity of the incident light. This creates the nonlinearity that we are modeling through BPM in MATLAB. The refractive index of the Kerr medium is given in the following equation

$$n = \bar{n} + n_2 I, \quad (2.10)$$

where n is the total refractive index, n_2 is the nonlinear refractive index and I is the intensity of the incident light. Angular propagation is modeled by multiplying the angle part to the phase component in the propagation step. In this simulation we have propagated a Gaussian beam through a certain distance in air then through a Kerr type nonlinear medium. The interface is modeled using the Fresnel transmission equation, so that after the interface we obtain the exact phase and amplitude components of the beam. The physical parameters used in the simulation are listed in the table below.

Physical Parameters	Value of the Physical Parameters
Wavelength of Incident Light (λ)	1.55 microns
Refractive index of the incident medium (n_0)	1 (air)
Average Refractive index of the Kerr medium (n)	3.5
Initial Peak Intensity of the Beam (I)	$10^{14} - 10^{16} \text{ W/cm}^2$
Nonlinear Refractive index or Kerr coefficient (n_2)	$10^{-16} \text{ cm}^2/\text{W}$
Angle of incident of the beam (θ)	$2 - 5^\circ$
Initial Beam Waist (w_0)	$10 \mu\text{m}$

Table 2.1 Beam and crystal parameters used in simulation of beam propagation in nonlinear Kerr medium.

2.4 Simulation Results

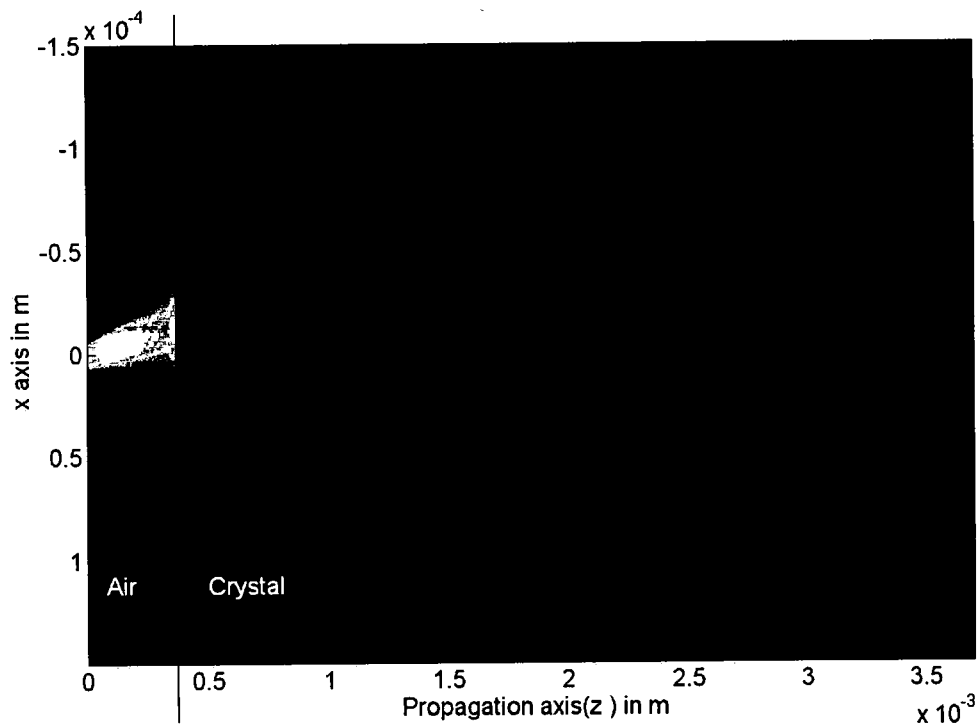


Figure 2.5a Almost linear propagation in nonlinear medium ($z_{\text{max}} = 30 z_r$).

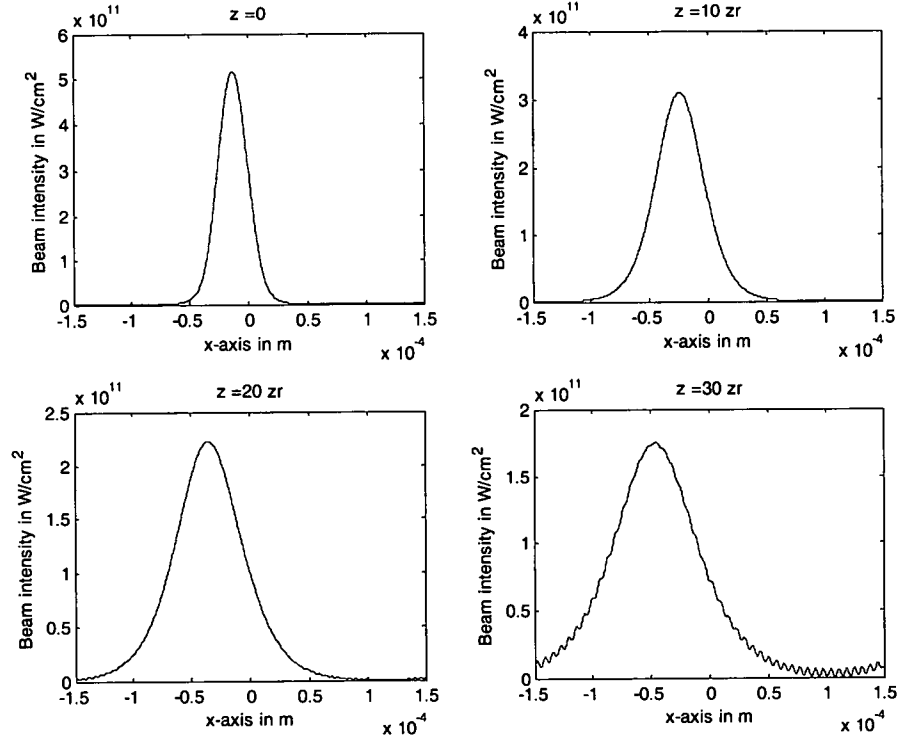


Figure 2.5b Almost linear propagation in nonlinear medium at various instants.

Figure 2.5 shows the propagation of a Gaussian beam in a Kerr medium which enters at an angle of 2 degrees with respect to z-axis, where the initial intensity of the beam is 10^{13} W/cm^2 . Also note that the beam propagates a distance of three Raleigh ranges before entering the medium. In this case the nonlinearity is almost negligible, giving rise to the almost linear propagation which has only diffraction effects and no appreciable focusing. When the initial beam intensity is $3.2 \times 10^{13} \text{ W/cm}^2$, we have an approximate (since initial profile is Gaussian) first order soliton where the beam remains same through out the propagation. If I_1 is the intensity for the first order soliton, then N^2 time I_1 will give rise to a N^{th} order soliton.

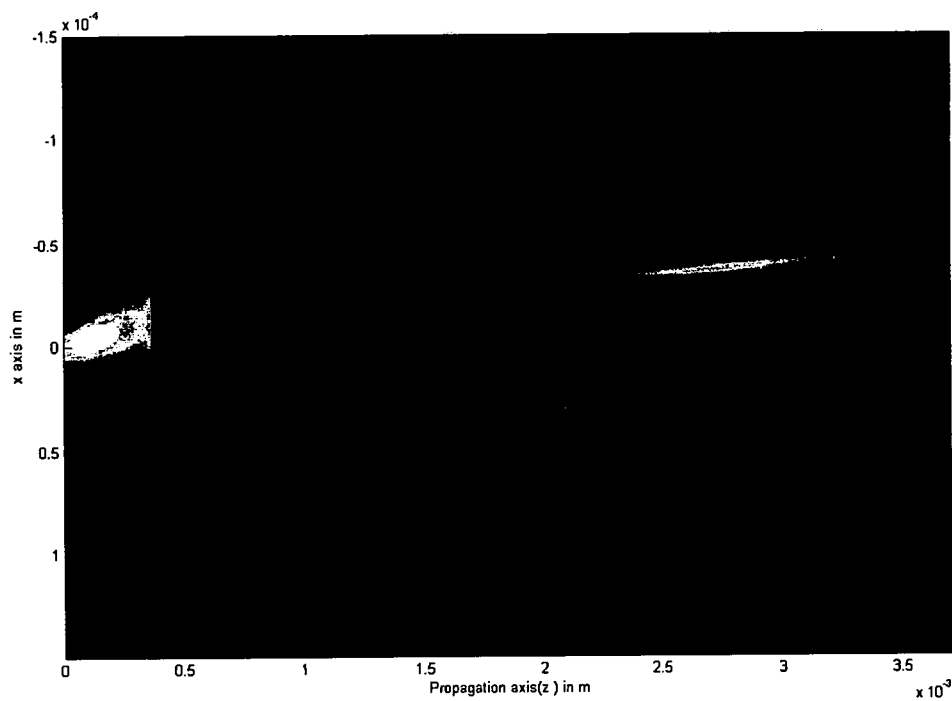


Figure 2.6a Self focusing in nonlinear Kerr media.

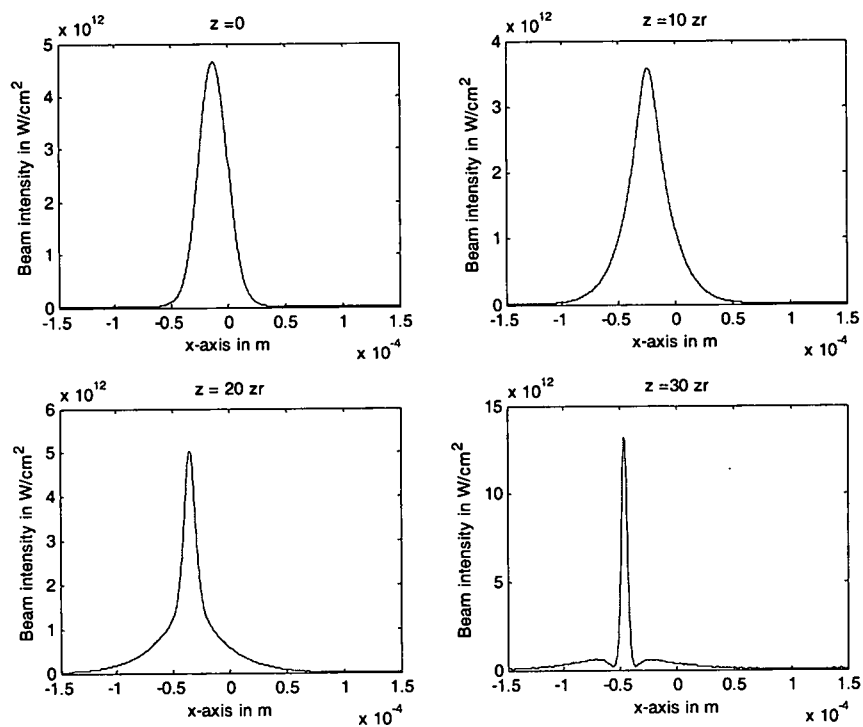


Figure 2.6b Self focusing profiles in nonlinear Kerr media at various distances.

When the initial intensity of the beam is around $9 \times 10^{13} \text{ W/cm}^2$, the increase in the intensity gives rise to the increase in the nonlinearity. This increase in nonlinear refractive index makes the beam self focus at a distance corresponding to the initial intensity. This is shown in Fig. 2.6. The self focusing is periodic, as shown in Fig. 2.7 for longer propagation. This is because up to a particular distance the beam converges due to nonlinearity and then start to expand due to diffraction. The self focusing distance for Kerr medium is given by the formula

$$f = \frac{w_b^2}{4n_2 I_n L}, \quad (2.11)$$

where w_b is beam waist inside the medium, I_n is the beam intensity inside the medium and L is length of the nonlinear medium. For the parameters tabulated in the table 2.1 the self focusing distance is calculated to be 2.9mm and our simulations are in accordance to the result.

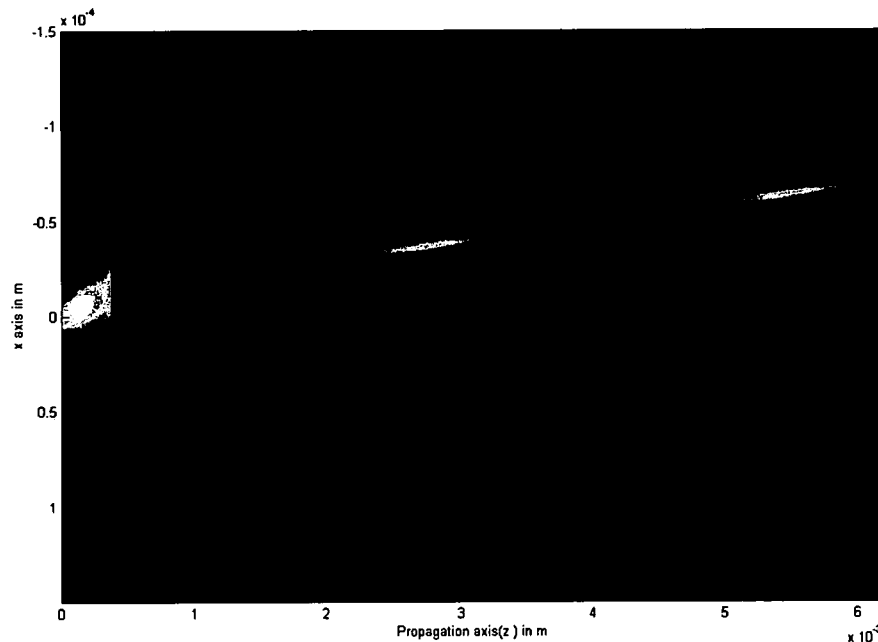


Figure 2.7 Periodic self focusing of Gaussian beam.

When we further increase the intensity of the beam to $17 \times 10^{13} \text{ W/cm}^2$, the beam self-focuses initially and then splits in two beams. This is called second order soliton propagation (see Fig. 2.8). Higher order Soliton propagation is achieved by the increasing the initial intensity to $25 \times 10^{13} \text{ W/cm}^2$. In third order soliton propagation the beam initially self focuses, then splits in to two and finally splits in to three (see Fig. 2.8 here the angle of propagation has been increased to 5 degrees). Note that periodic self-focusing and splitting happen in second order and third order solitons. The MATLAB simulation code for angular Gaussian beam propagation in nonlinear Kerr media is presented in Appendix.

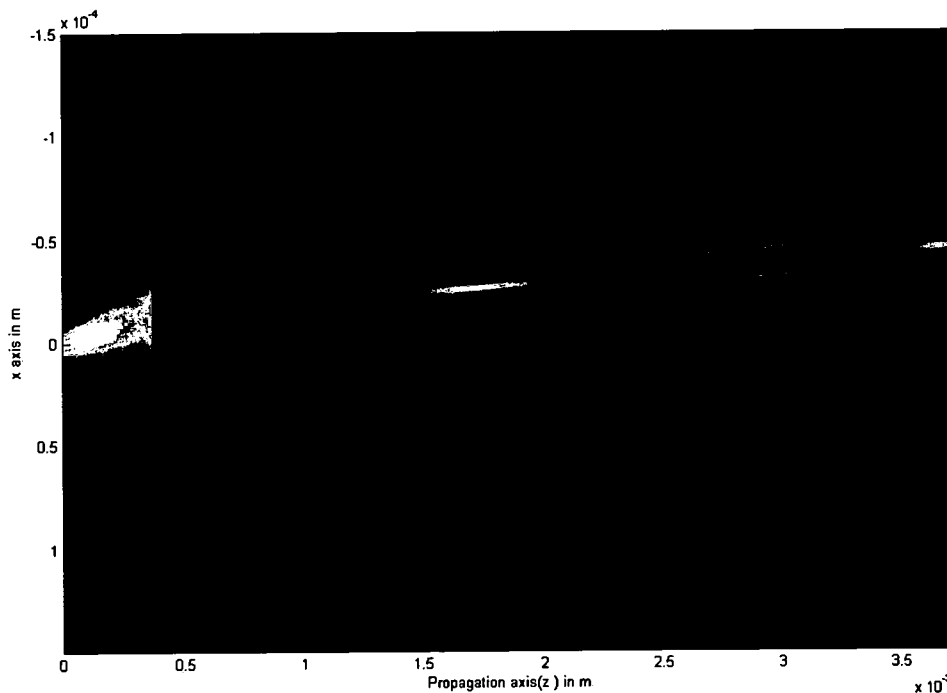


Figure 2.8a Second order soliton propagation.

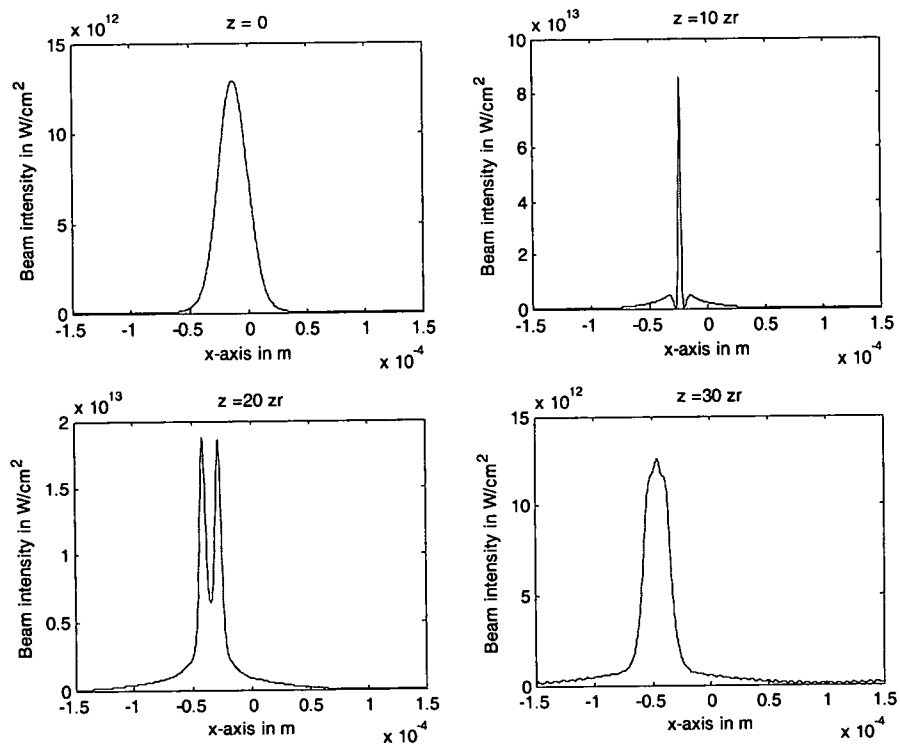


Figure 2.8b Second order soliton profiles at various distances.

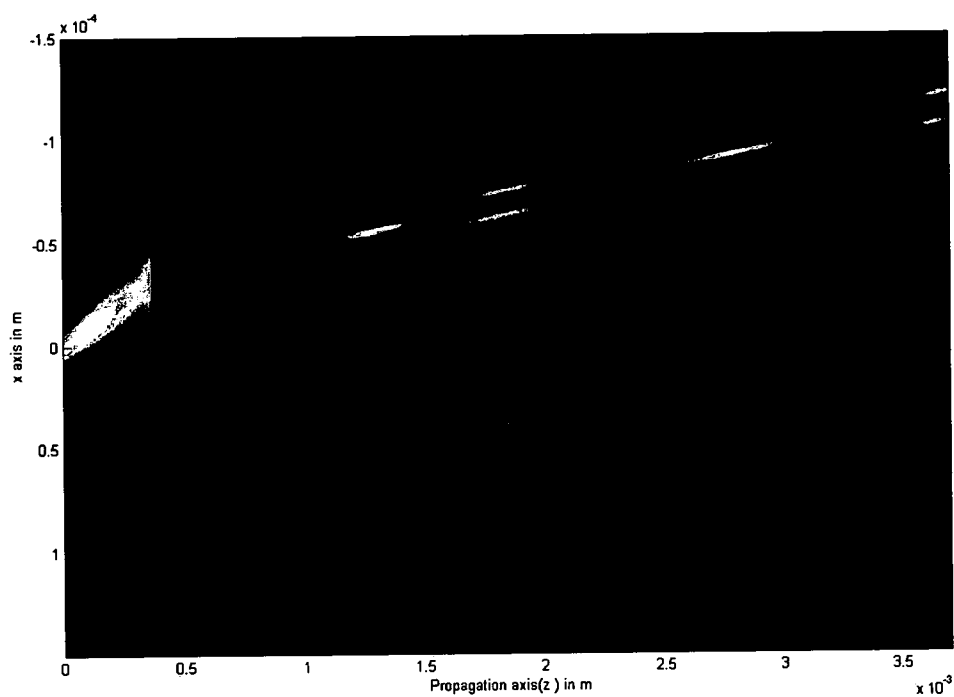


Figure 2.9a Third order soliton propagation.

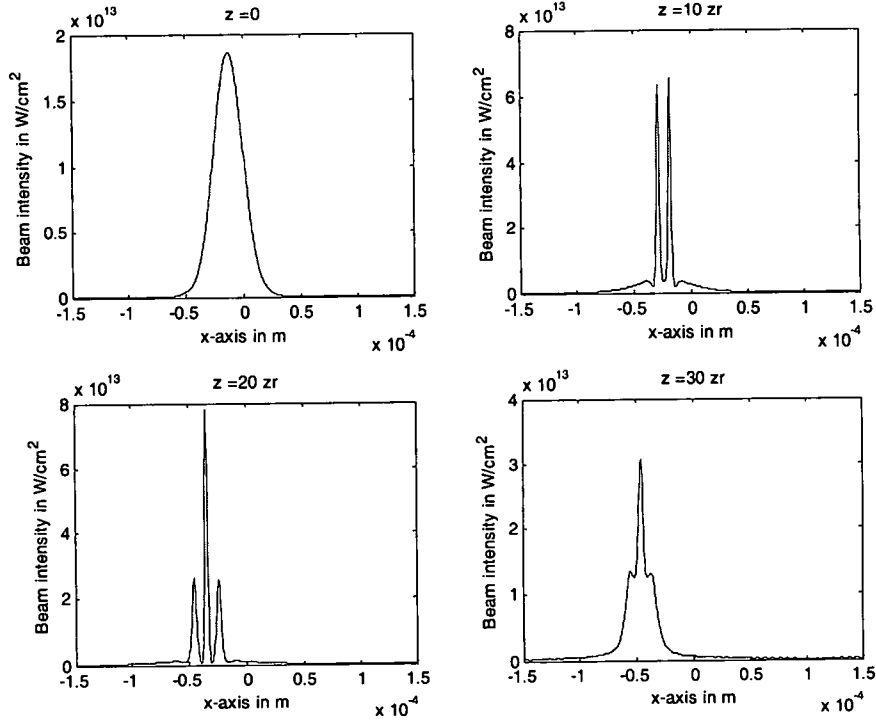


Figure 2.9b Third order soliton profiles at various distances.

2.6 Conclusion

In this Chapter we have discussed the well know BPM using FFT. We have applied this technique to simulate beam propagation in well studied nonlinear Kerr media. This development here will be used in the next Chapter to simulate Gaussian beam propagation in a PR medium, where the induced change in refractive index is proportional to the gradient of the intensity for a diffusion-dominated material.

Chapter 3

Distinction between Deterministic and Random Beam Fanning in Photorefractive Materials

3.1 Introduction

Beam fanning can be classified into two kinds; RBF and DBF. RBF is caused due to the amplification of scattered light by two wave mixing. This scattering occurs due to inhomogeneities or imperfections at the surface or in the bulk of PR crystals. On the other hand DBF as suggested by Banerjee and Misra [1] is caused due to an asymmetric refractive-index profile created by a symmetric beam in a diffusion dominated material such as BaTiO_3 , or a symmetric refractive index profile in photovoltaic materials such as LiNbO_3 . In this Chapter we review the theory of beam fanning by first presenting the derivation of set of expressions for the induced refractive index change from the Kukhtarev equations. Through simulation results using the BPM, we discuss the effect of various beam and material parameters on the occurrence of RBF and DBF. In the process, we also find the conditions under which one is more dominant than the other.

3.2 Induced Refractive Index Change in PR Media

The Kukhtarev equations presented in Chapter 1 is coupled set of differential equation. By performing a steady state analysis for the these equations we can get the ordinary differential equation for the space charge field E_s as

$$\nabla^2 E_s = \left(\frac{eN_a}{\epsilon_s} - \nabla \cdot E_s \right) \left(\frac{eE_s}{k_B T} - \frac{\nabla I}{\left(\frac{\beta}{s} + I \right)} \right), \quad (3.1)$$

where e is the electronic charge, N_a is the acceptor concentration, ϵ_s is the electrostatic permittivity, k_B is the Boltzman constant, T is the temperature, $I \propto |E_s|^2$ is the intensity of the optical field, β is the dark current and s is the ionization cross-section. An approximate solution for the above equation is

$$E_s \approx \frac{k_B T}{e} \frac{\nabla I}{\left(\frac{\beta}{s} + I \right)} = E_{sx} a_x + E_{sy} a_y, \quad (3.2)$$

provided $W^2 \gg \epsilon_s k_B T / e^2 N_A$, where W is the characteristic width of the envelope E_e of the optical field, and a_x, a_y are unit vectors in the x and y directions respectively.

Let us consider the case of BaTiO_3 , where the electrostatic field as given in Eq. (3.2) induces a refractive change via the linear electrooptic effect. The grating formation here is due to a single incident beam. Energy exchange between different angular plane wave spectra of the beam and/or scattered waves (from surface and/or volume inhomogenties or imperfections) occur via two wave mixing. Restricting

ourselves for now to one transverse dimension, the index change for an incident extraordinary polarized light is given as

$$\Delta n_{ext}(x, z, \theta) = E_x(x, z) f(\theta), \quad (3.3)$$

$$f(\theta) = -\frac{1}{2}n_e^3(\theta)\cos\theta \times (r_{13}\sin\theta + r_{33}\cos^2\theta + 2r_{42}\sin^2\theta), \quad (3.4)$$

$$n_e^2(\theta) = \left(\frac{\cos^2\theta}{n_e^2} + \frac{\sin^2\theta}{n_o^2} \right)^{-1}, \quad (3.5)$$

where n_o, n_e are the linear ordinary and extraordinary refractive indices, respectively, r_{ij} are the linear electrooptic coefficients, and θ is the angle between x axis and the c -axis of the crystal within the material. The evolution of the envelope of the optical beam in the material can be modeled by applying slowly varying envelope approximation as

$$\frac{\partial E_e}{\partial z} = -ik_0\Delta n_{ext}E_e - i\left[\frac{1}{2n_e^3(\theta)k_0}\right]\nabla_{\perp}^2 E_e, \quad (3.6)$$

$$\Delta n_{ext}(x, \theta) = F_x^{-1}\left[F_x[E_x(x)] f\left(\frac{k_x}{n_e(\theta)k_0} + \theta\right)\right], \quad (3.7)$$

$$E_{sx}(x) = \frac{k_b T}{e} \left[\frac{\frac{\partial |E_e|^2}{\partial x}}{\frac{n\beta}{s} + |E_e|^2} \right]. \quad (3.8)$$

In Eqs. (3.6)–(3.8) k_0 is the propagation constant in vacuum and η is the characteristic impedance of the material. Note that k_x is the spatial frequency in the x direction.

3.3. Simulation of DBF

In this Section, we first present a typical result of the analysis of DBF in PR BaTiO₃ to corroborate our simulations with earlier results. DBF is characterized by the shift and appearance of side-lobes due the asymmetric refractive index profile created by a symmetric beam. The amount of DBF is defined by the relative amount of power in the side lobes. The factors that have been analyzed are the peak intensity of beam, beam width, c- axis orientation and angle of incidence. For simulation we consider a Gaussian

input $E_{in}(x) = (I_0\eta)^2 \exp\left[-\frac{(x^2)}{W^2}\right]$ where I_0 is the on-axis intensity which is given by

the formula $I_0 = \frac{2P}{\pi W^2}$, P is the power beam power and W is the width (waist) of the

beam. We use the BPM technique for the propagation of beam and the calculation of induced refractive index grating due the intensity. In essence BPM incorporates diffraction and (induced) refraction done in two consecutive steps. In the first step we obtain the plane wave spectrum (through FFT in MATLAB) and multiply it with the propagation phase. In the second step we go back to the space domain and multiply the phase correction required for the inhomogeneities or nonlinearity in the medium. This step is repeated until we propagate the beam to desired distance. The refractive index change is calculated based on Eq. (3.7) along with Eqs. (3.4), (3.5) and (3.8) for every propagation step. After considerable propagation in the crystal the optical field is phase modulated. This phase modulation results in the asymmetry and side lobe formation which is amplified during further propagation in the crystal.

For numerical simulation we consider a BaTiO₃ crystal with following parameters. $T = 300 \text{ K}$, $\beta = 2\text{s}^{-1}$, $n_o = 2.488$, $n_e = 2.434$, $r_{42} = 1640 \text{ pm/V}$, $r_{13} = 8 \text{ pm/v}$, $r_{33} = 28 \text{ pm/v}$, $s = 2.6 \times 10^{-5} \text{ m}^2/\text{J}$, $N_A = 2 \times 10^{22} \text{ m}^{-3}$, $\eta = 377 \text{ ohms}$. The beam parameters used are initial beam waist $W = 8 \text{ microns}$, incident angle $= 1 \text{ degree}$, wavelength $\lambda = 0.532 \text{ microns}$ (green), input laser power $P = 1.6\text{mW}$, angle between incidence and c-axis $\theta = 55^\circ$, and thickness of the crystal $L = 1\text{cm}$. It is also assumed that the beam propagates a Raleigh range before incidence onto the crystal. The above parameters are the default parameters for numerical simulation in this Chapter; if a change of parameter is made, it is stated specifically.

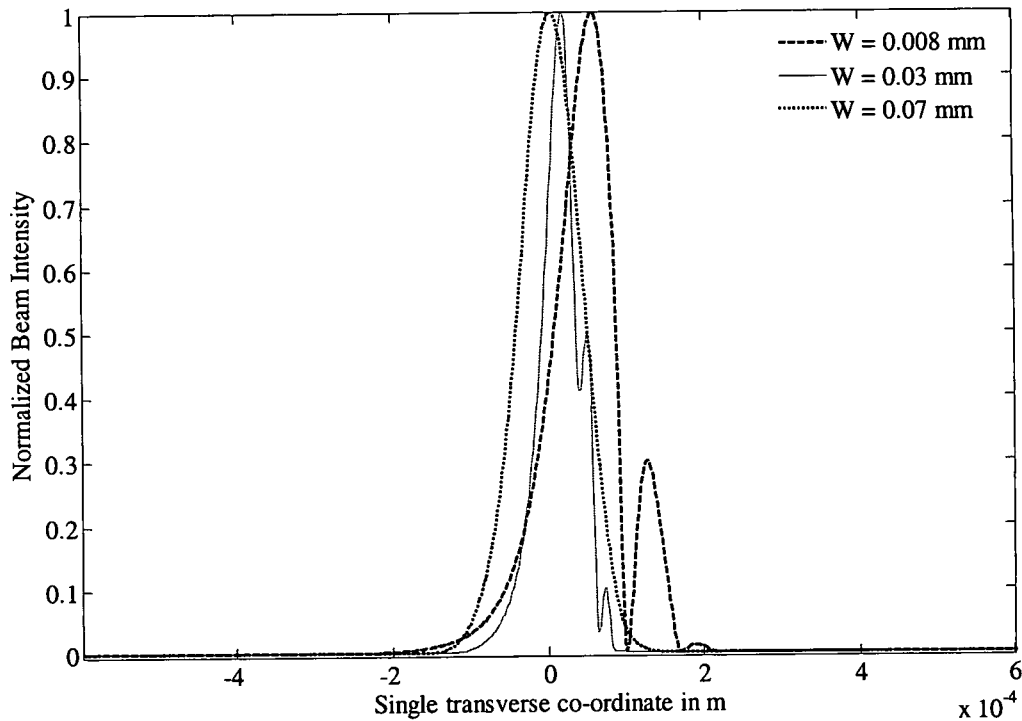


Figure 3.1 Normalized intensity profile at the exit of the crystal for various beam waists.

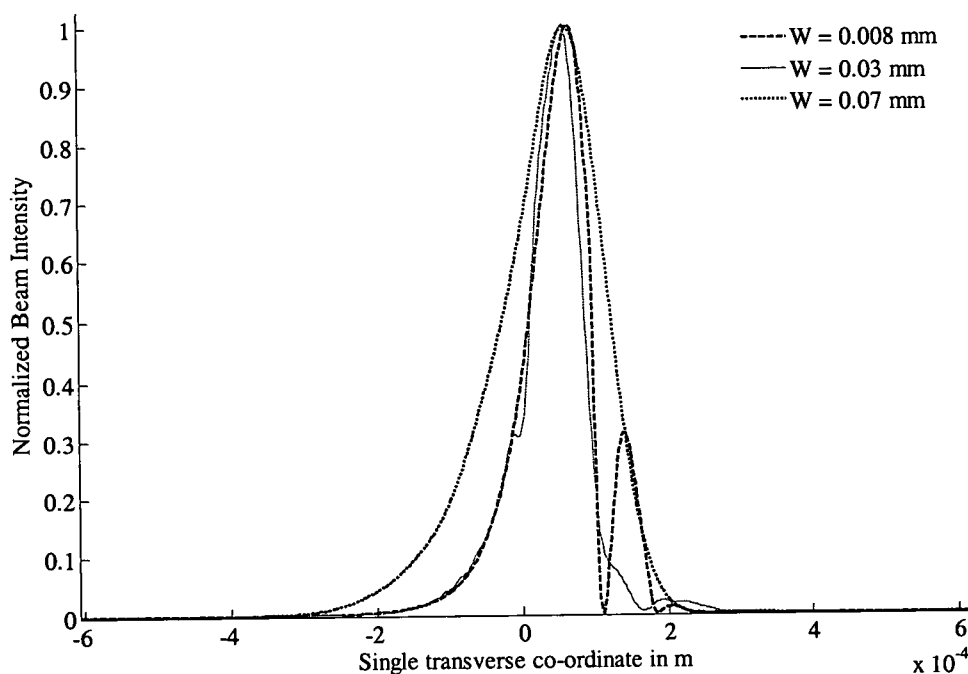


Figure 3.2 Normalized intensity profile at far field for various beam waists.

Figures 3.1 and 3.2 show the effect of beam waist on DBF. DBF can be noticed for waist of $5\mu\text{m}$ to $70\mu\text{m}$. It is more prominent around $8\mu\text{m}$ to $40\mu\text{m}$ beam waist region and peaks around $W = 25\mu\text{m}$. By prominent we mean, the appearance of side lobes can be clearly spotted. In rest of the DBF region, although side lobes are not seen the shift can be evidently noticed. Next in order to see the effect of beam power in DBF, we vary the beam powers from 0.2mW to 10mW . As shown in Figs. 3.3 and 3.4, over the range of powers used, we observe DBF effects to keep increasing. The angle between c-axis and the propagation direction also affects DBF. As shown in Fig. 3.5, DBF increases with increase in the angle but it peaks around 55 degrees, thereafter reducing as we further increase the angle. The reason for the maximum at 55 degrees is due to the maximum induced change in refractive index at this angle for the chosen values of the electro-optic

coefficients. In Fig. 3.4, The sample has been approximated as a “thin” sample, meaning that diffraction effects within the sample has been neglected. This approximation in general can be valid if W is larger than tens of microns for sample length of 1 cm.

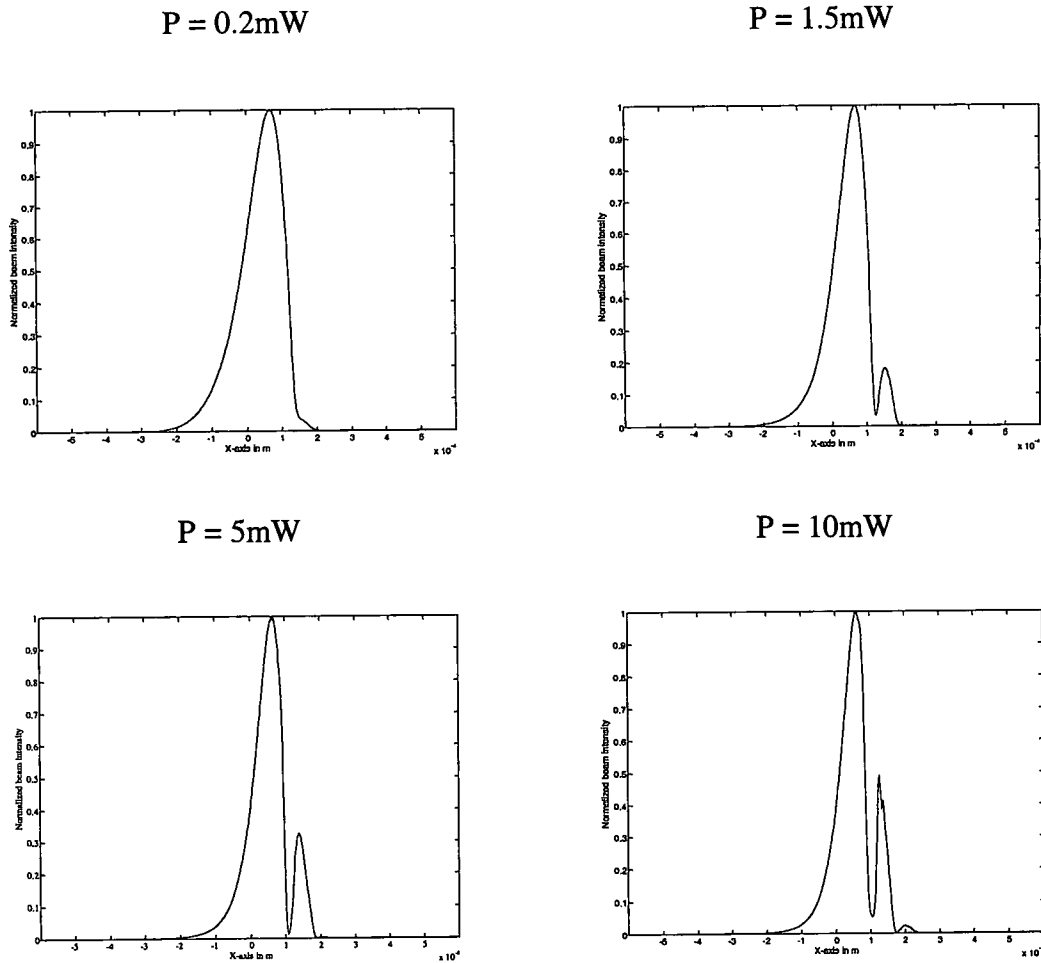
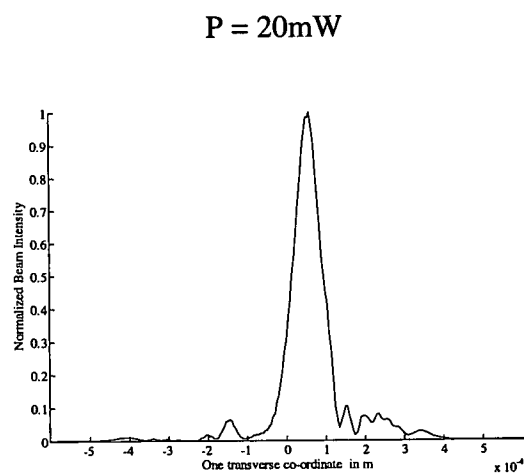
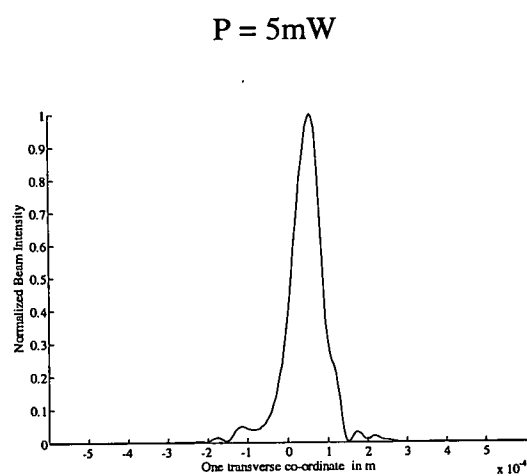
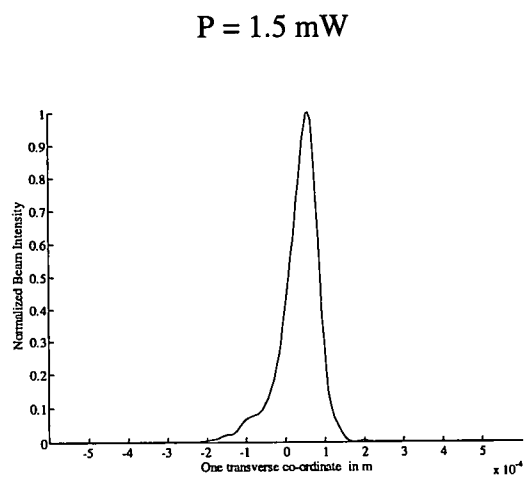
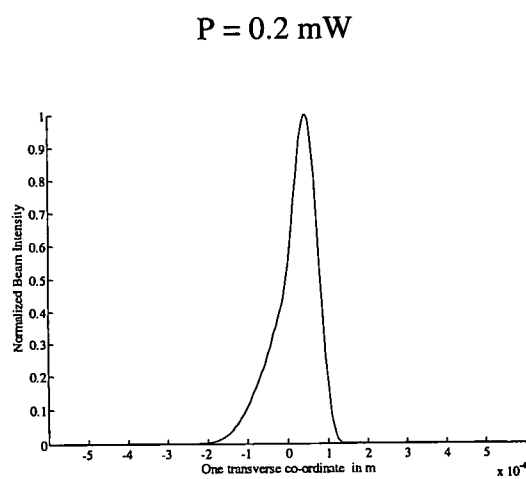


Figure 3.3 Normalized intensity profile at far field of thick sample for various power levels (Beam Width = $8\text{ }\mu\text{m}$ and sample length = 1 cm).



*Figure 3.4 Normalized intensity profile at far field of thin sample for various power level
(Beam Width = $40 \mu\text{m}$ and sample length = 1 cm).*

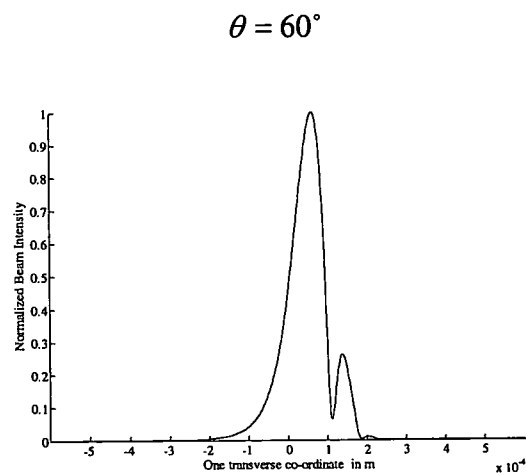
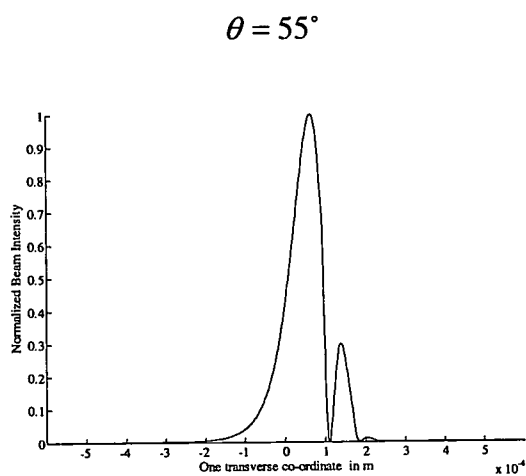
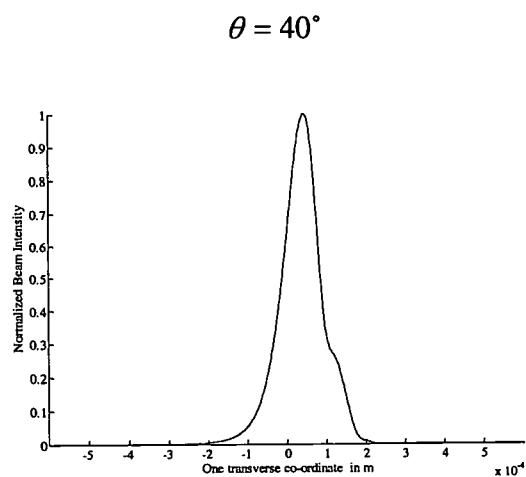
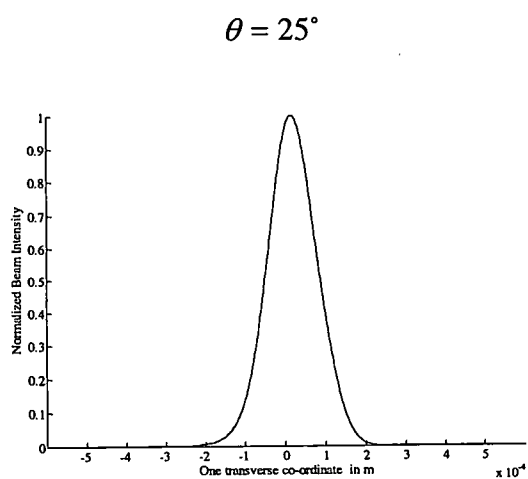


Figure 3.5 Normalized intensity profile at far field for various X-cut crystals (Beam Width = $8\ \mu\text{m}$ and sample length = 1 cm).

3.4. Incorporation of RBF

RBF arises from the scattering of light from inhomogeneities on the surface of and in the bulk of the crystal. First, a very small portion of the incident beam may be scattered from inhomogeneities and impurities at the crystal surface. The remaining part of the incident beam interacts with the scattered parts via two-wave mixing. This leads to an amplification of the scattered light in the direction of the energy transfer. RBF has been analyzed extensively in the literature [34-35]. The inhomogeneities and impurities that give rise to RBF may also persist in the bulk of the crystal. These impurities are random in nature, so they can give rise random modulation of both phase and intensity. These modulations are modeled by including random phase and intensity terms to the optical field. These terms are included when the beam strikes the crystal surface and also in every propagation step. The intensity and phase of the randomness can also be varied in our numerical simulations. Fig. 3.6 shows the simulation of RBF for a beam waist (W) of 100 microns and where the inhomogeneities are introduced at intervals of 4 microns in the transverse dimension with randomness of 10^{-11} both in amplitude and phase components of the beam. We remark that similar results are also observed with only surface randomness, whose amplitudes are made equal to the total accumulated randomness the beam encounters while propagating through the sample.

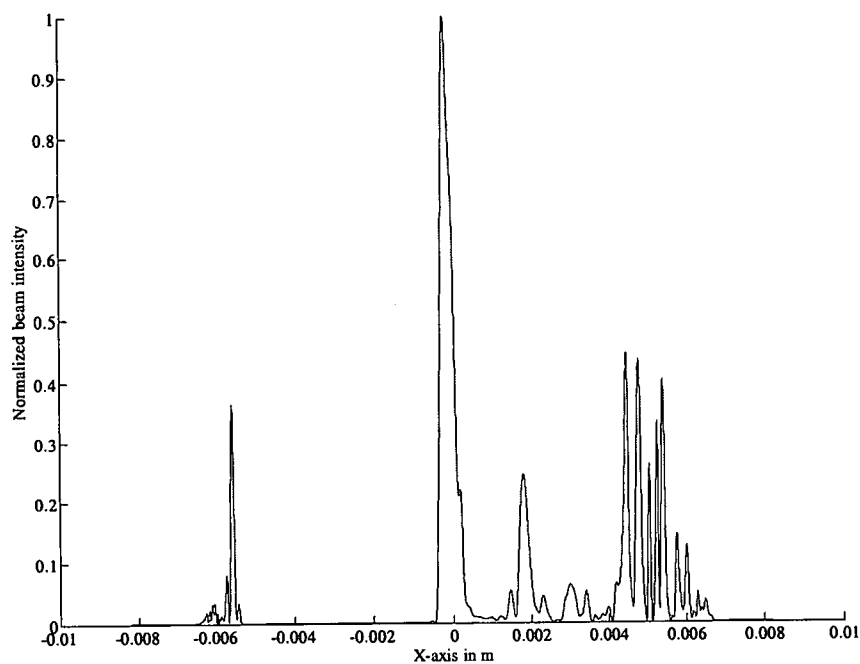


Figure 3.6a Normalized beam profile at far field for BaTiO₃ crystal.

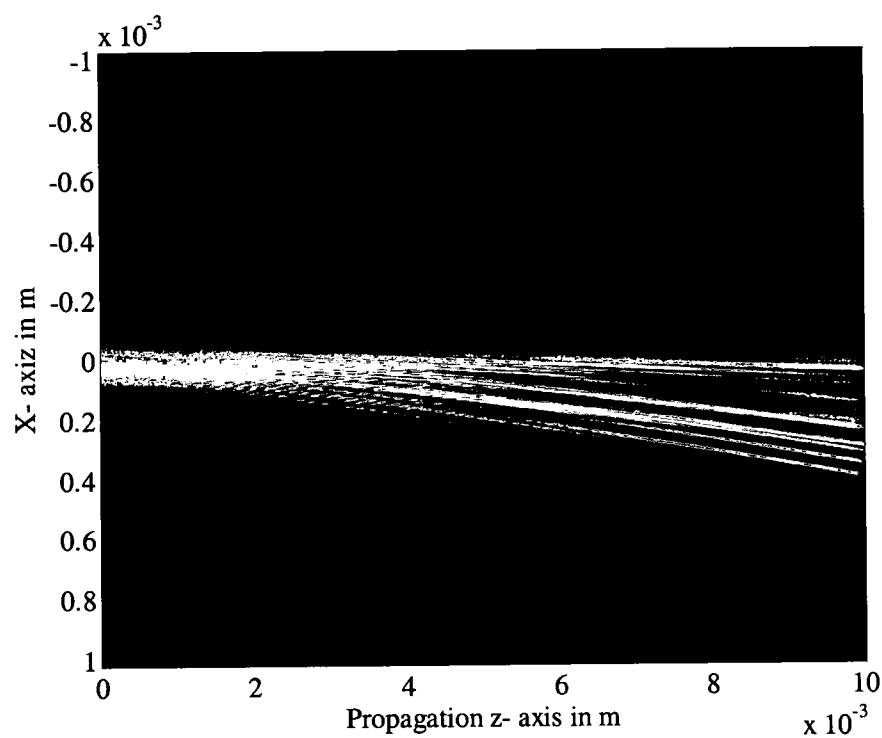


Figure 3.6b Simulation of beam propagation in BaTiO₃ crystal giving rise to RBF.

3.5. Effect of Beam Waist on Beam Fanning

DBF and RBF occur together and for the same reason in PR media. But in certain cases DBF may dominate and in other cases RBF may be more prominent. We find that beam waist plays a major role in determining the kind of fanning. For values of beam waist around 8 microns to 50 microns, the fanning is predominantly DBF, while above 60 microns it is predominantly RBF (see, for instance, the sequence of Figs 3.7-3.9. Thicker beams give rise to more RBF because they illuminate more inhomogeneities and these scattered parts get amplified easily.

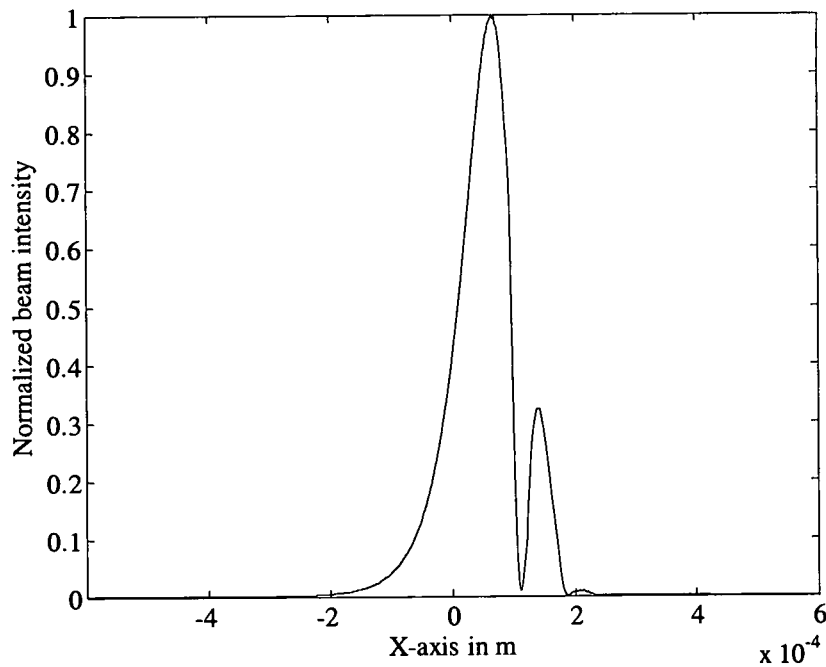


Figure3. 7a Normalized beam intensity at far field for BaTiO₃ ($W = 8$ microns).

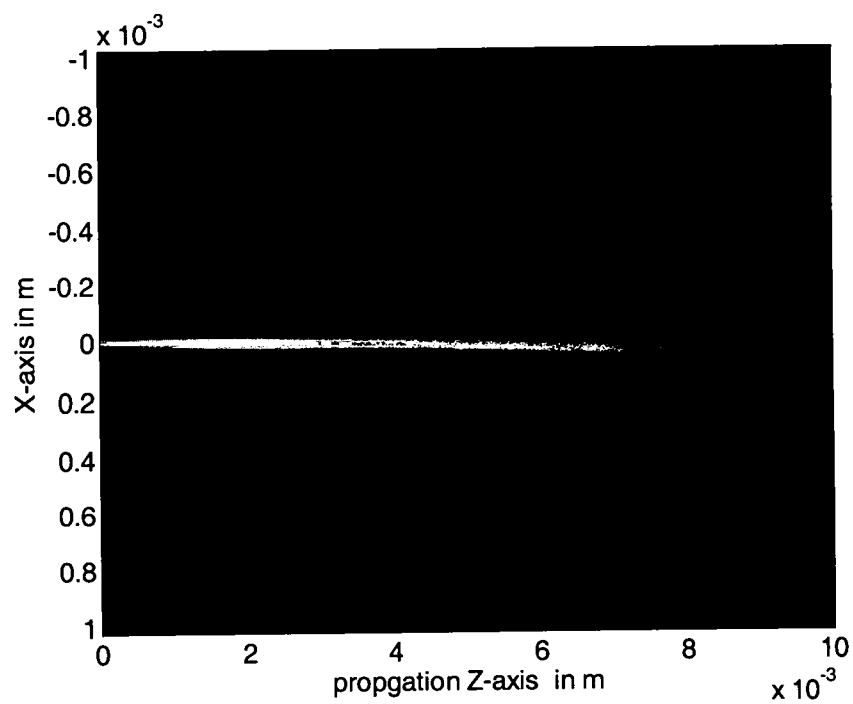


Figure 3.7b Simulation of beam propagation in BaTiO_3 crystal ($W = 8$ microns).

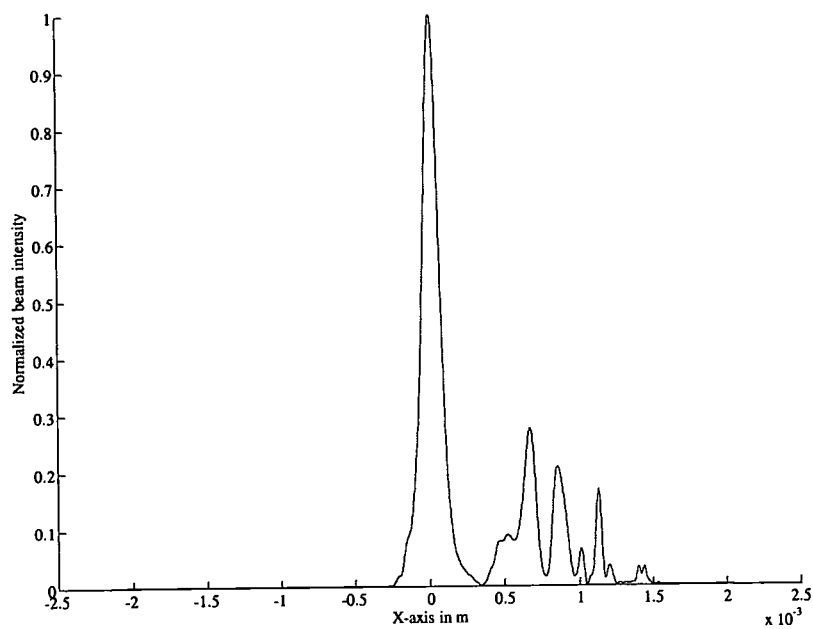


Figure 3.8a Normalized beam intensity at far field for BaTiO_3 ($W = 50$ microns).

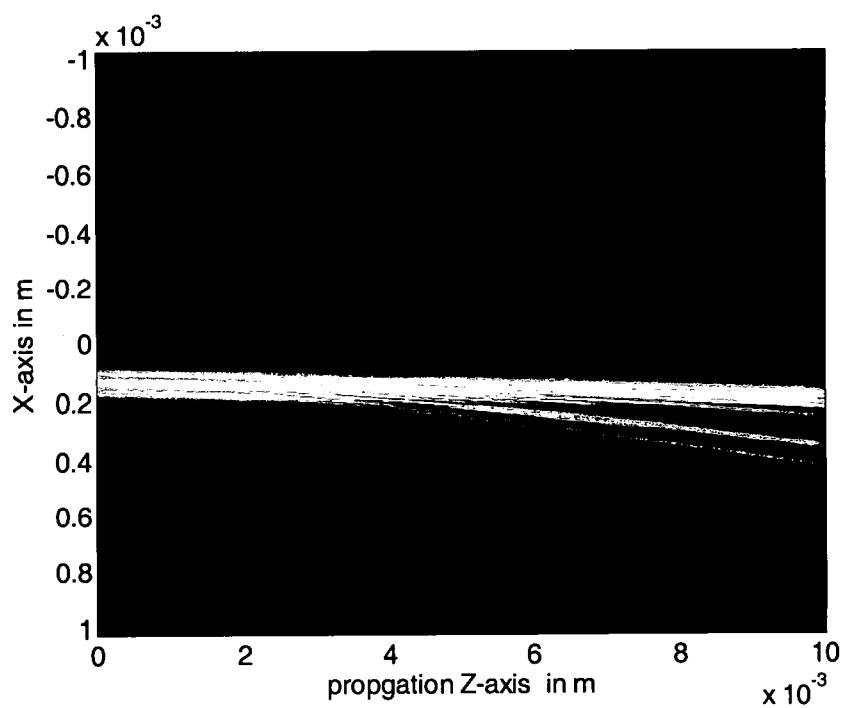


Figure 3.8b Simulation of beam propagation in BaTiO₃ crystal ($W = 50$ microns).

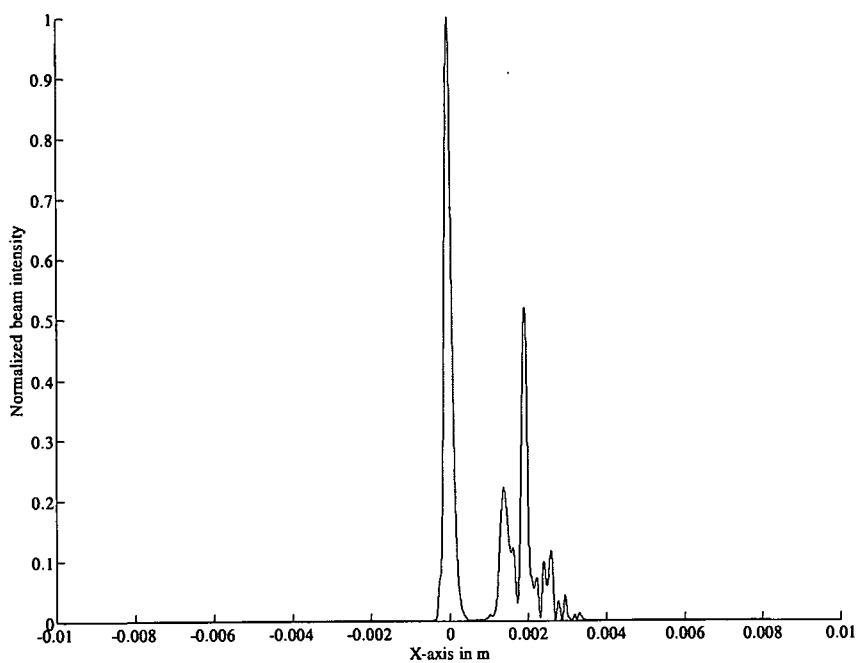


Figure 3.9a Normalized beam intensity at far field for BaTiO₃ ($W = 80$ microns).

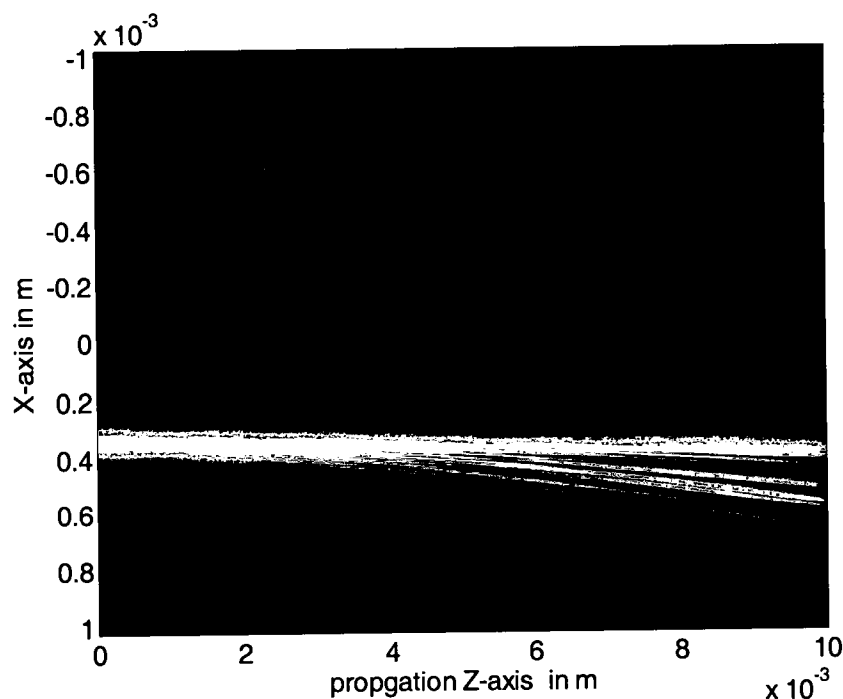


Figure 3.9b Simulation of beam propagation in BaTiO_3 crystal ($W = 80$ microns).

3.6. Effect of Randomness on Beam Fanning

As expected, the amount of randomness determines the amount of RBF. When we increase the randomness by an order the RBF increases and if we decrease it by an order, RBF decreases and/or the fanning becomes predominantly DBF. Increase in the magnitude and decrease in the spacing of randomness will lead to more RBF, as seen in Fig. 3.10 where the noise interval is reduced to 2 microns (from 4 microns) and amount of randomness in both amplitude and phase is increased to 10^{-10} . (from 10^{-11}). The increase in the randomness is evident when compared to Fig. 3.9. On the other hand, as seen from Fig. 3.10, when the randomness is decreased by an order, the fanning changes from RBF to DBF.

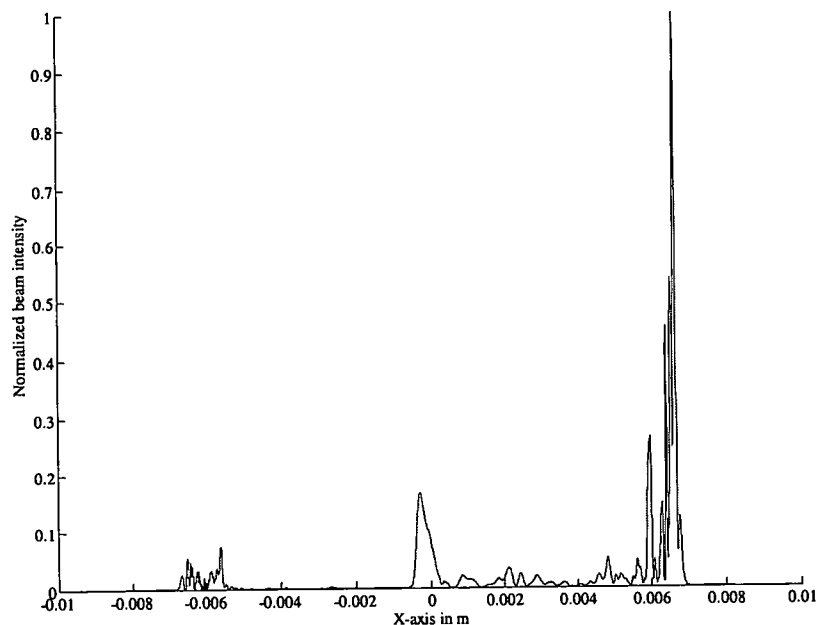


Figure 3.10a Normalized beam intensity at far field for BaTiO_3 ($W = 100$ microns) with increased randomness.

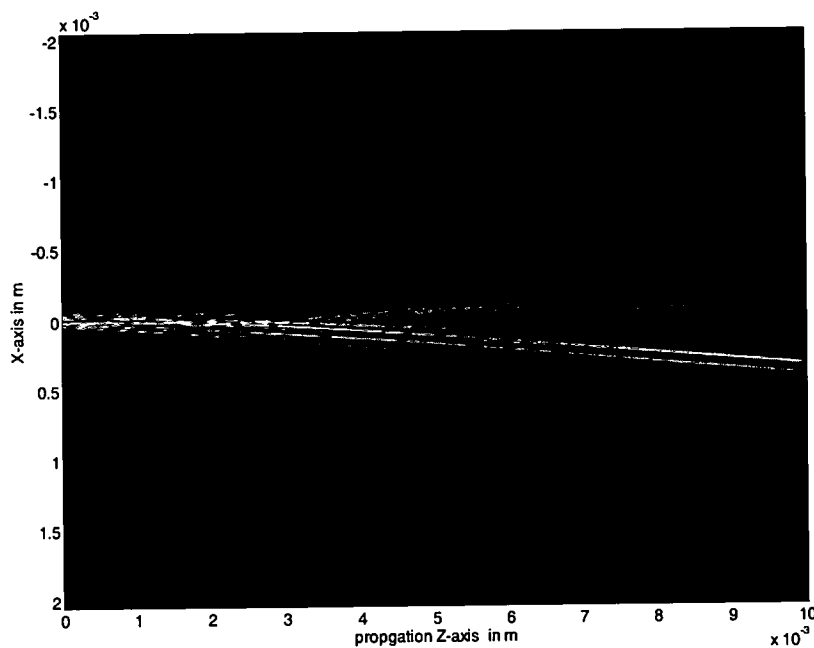


Figure 3.10b Simulation of beam propagation in BaTiO_3 crystal ($W = 100$ microns).

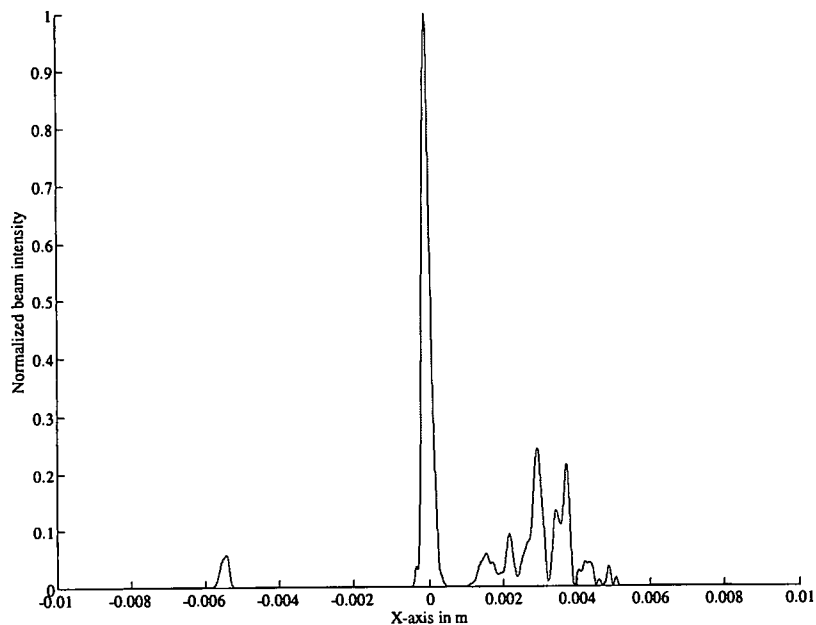


Figure 3.11a Normalized beam intensity at far field for BaTiO_3 ($W = 100$ microns) with decreased randomness.

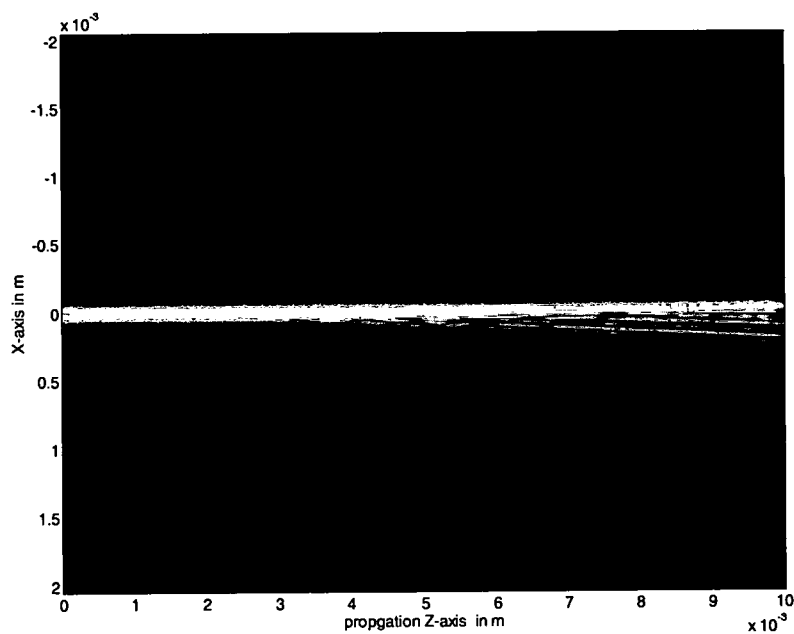


Figure 3.11b Simulation of beam propagation in BaTiO_3 crystal ($W = 100$ microns) with decreased randomness.

3.7 Effect of Length of Sample in Beam Fanning

Sample length affects the fanning. As the length increases, the product of the gain coefficient and length increases, as also the inhomogeneities seen by the beam, thus giving rise to increased RBF. When the sample size is reduced to 0.5 cm for a 100 micron beam, the fanning changes from RBF to DBF (see Fig. 3.12), while when the sample size is increased to 2 cm for 100 micron beam, the fanning increases (see Fig. 3.13).

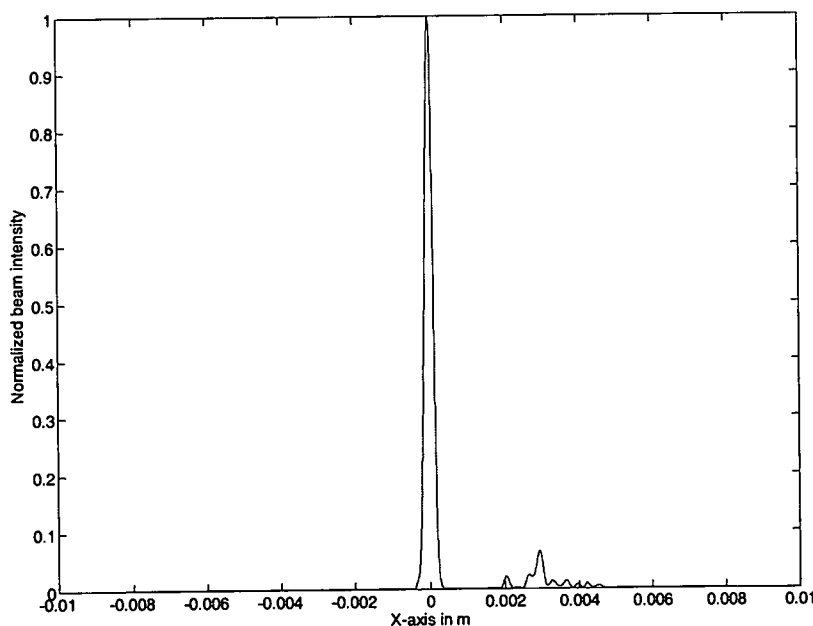


Figure 3.12a Normalized beam intensity at far field for BaTiO₃ (W = 100 microns) with sample length 0.5 cm.

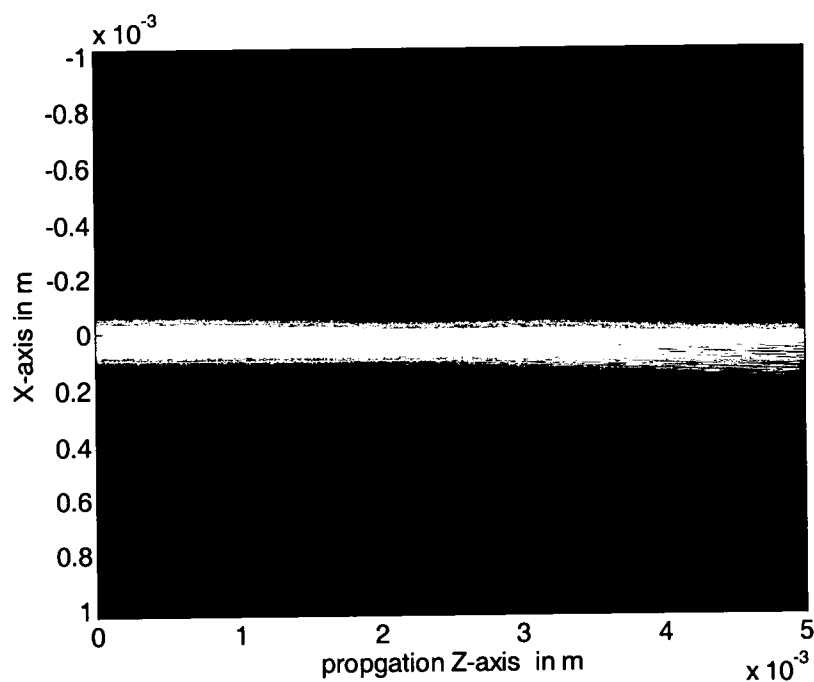


Figure 3.12b Simulation of beam propagation in BaTiO_3 crystal ($W = 100$ microns) with sample length 0.5 cm.

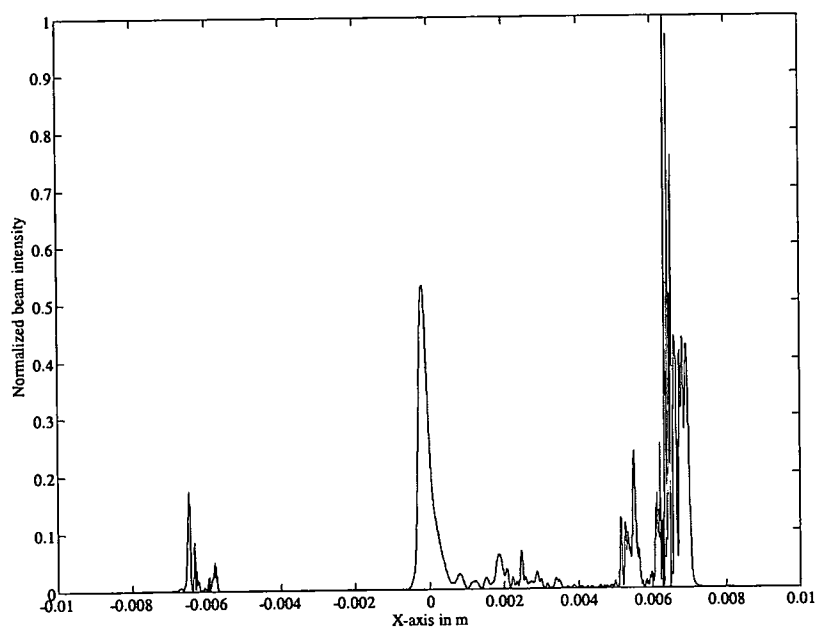


Figure 3.13a Normalized beam intensity at far field for BaTiO_3 ($W = 100$ microns) with sample length 2 cm.

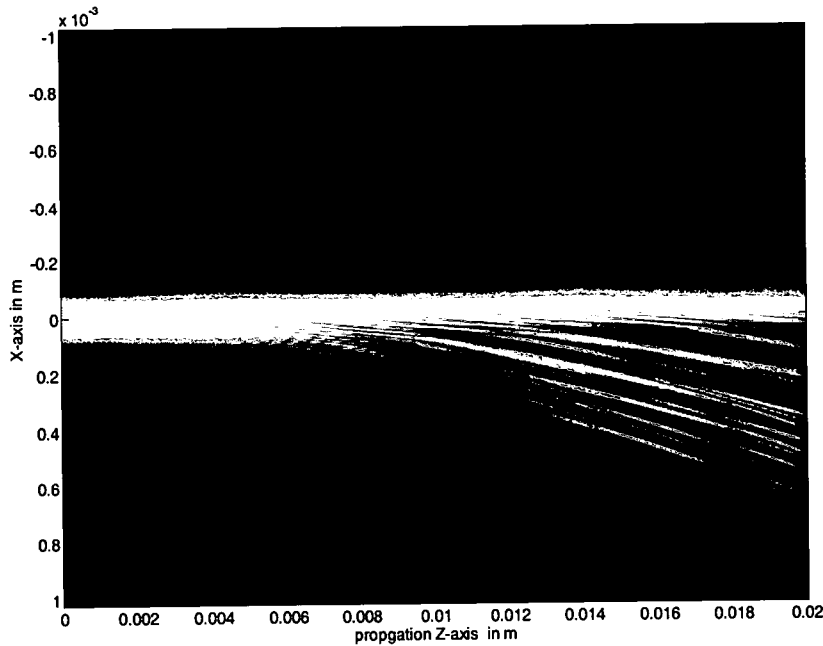


Figure 3.13b Simulation of Beam propagation in BaTiO₃ crystal ($W = 100$ microns) with sample length 2 cm.

3.8. Summary

In summary, we have presented the theory of DBF and RBF in nonlinear PR media. We have extensively analyzed the factors that give rise to DBF and RBF in diffusion dominated material like BaTiO₃. The factors affecting fanning are beam waist, power, inhomogeneities, and the sample thickness. Also, fanning is the highest when the c-axis is about 55 degrees w.r.t. the transverse axis. By introducing random surface and bulk inhomogeneities in the crystal, we have analyzed the occurrence of DBF and RBF. We conclude that DBF is dominant for lower beam waists in order of tens of microns, smaller sample length and smaller random inhomogeneities. Precise determination of

which type of fanning, DBF or RBF, will dominate can be determined explicitly using our developed technique and is listed in Table 3.1.

Parameters	DBF	RBF
Beam Width	8 to 50 μm	> 70 μm
Beam Power(1.5mw is enough for fanning)	Increases fanning but stays as DBF	Increases the Fanning
C- axis orientation and Angle of incidence	Increase till 55° then decreases	Increase till 55° then decreases can become DBF if its too low
Randomness intensity	< 10^{-11}	> 10^{-10}
Randomness spacing	> 4 microns	< 2 microns
Length of sample	< = 1cm	>= 1cm
Wavelength of the Beam	Fanning decreases with increase in wavelength	Fanning decreases with increase in wavelength

Table 3.1 Distinction between DBF and RBF.

Chapter 4

Simulation of Phase Conjugation in PR Media and Conclusion

4.1 Introduction

In Chapter 3 we have performed a detailed analysis of random and DBF in diffusion dominated PR media. One other phenomenon common in PR media is phase conjugation. Phase conjugation in PR media can occur in various configurations. In this Chapter we discuss the simulation of two such configurations: Phase conjugation through scattering from the back surface of the crystal and other is from mutual beam mixing of two Gaussian beams traveling in opposite directions through induced transmission gratings as discussed in Chapter 1. Further we also discuss the possibilities of future work and some useful conclusions based on this work.

4.2 Simulation of Phase Conjugation in PR via Backscattering

Propagation of coherent beam writes gratings in the PR media. These gratings change continuously as long as the beam is incident and reaches a steady state after a certain time. This grating formation sometimes gives rise to phase conjugation in the

back scattered beam. The logical next stage to the previous Chapter is to investigate the appearance of phase conjugation in back scattered beam.

To simulate back scattering we need to incorporate two more aspects in the algorithm used in Chapter 3 to simulate beam fanning: one is the reflection of beam from the back crystal-air interface and the other is continuous change of refractive index profile in the medium. The reflection is modeled by adding Fresnel reflection coefficients for every plane wave component at the interface. As the reflected light intensity is less than 10 percent of the incident light, only two reflections have been considered. When we propagate in the forward direction we store the refractive change in the medium in a matrix and use it as the refractive index profile seen by the reflected beam. The reflected beam adds its own grating to the previous existing grating, thus we add the new refractive index to the old refractive index profile. Now the next forward propagating beam sees this new refractive profile and it recreates its own profile. We carried this process for more than five thousand space steps and several round trips. As we see from our simulations, a true phase conjugate beam does not form. The reason for this is possibly that we did not provide for sufficient overlap between the forward and backward traveling beams for significant coupling between gratings created by the forward and backward traveling beams. Traditionally, researchers have relied on corner reflection to explain fanning generated phase conjugation.

We have checked for the phase conjugation using the following reasoning. A beam is said to be phase conjugated if we can reverse the beam both in direction and phase. So, in case of angular propagation the phase conjugate part of backscattered beam will trace the incident path in the opposite direction. Moreover over the phase conjugate

will converge to the source point of the beam. But the non-phase conjugate part of the beam should follow Fresnel reflection and continue to diverge. Simulation results for 80 micron beam with an angle of incidence 3 degrees for single pass is shown in Fig. 4.1 and for ten passes is shown Fig. 4.2. Further we have analyzed this configuration by changing the parameters like beam waist, beam power, c-axis orientation, angle of incidence and randomness in the medium. This also does not produce any phase conjugation. Thus we conclude that phase conjugation via backscattering cannot be explained using the band transport model and reflection from only the back surface of the crystal.

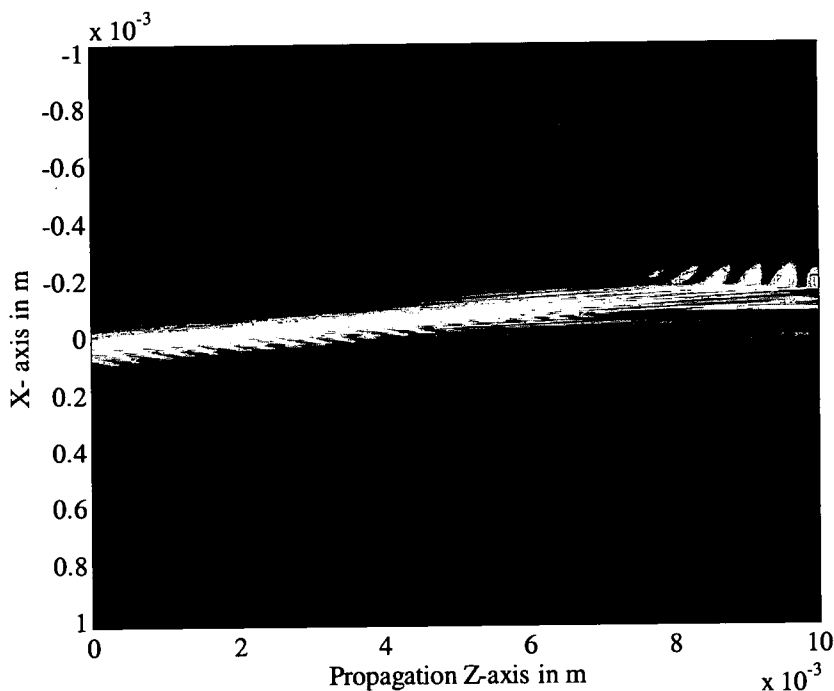


Figure 4.1a Incident and backscattered beam for one pass.

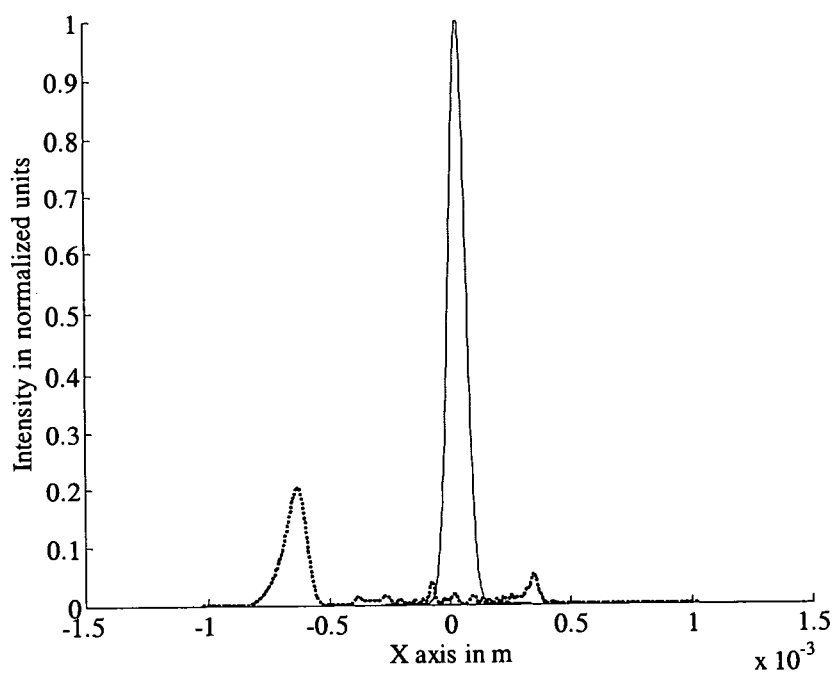


Figure 4.1b Backscattered beam (dotted) and original beam at the initial position for one pass.

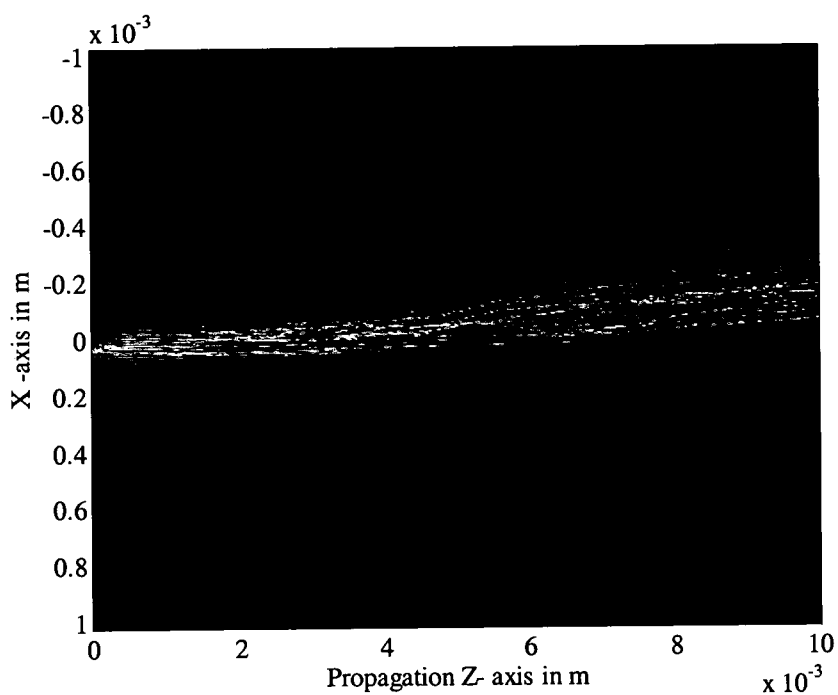


Figure 4.2a Incident and backscattered beam for 10 passes.

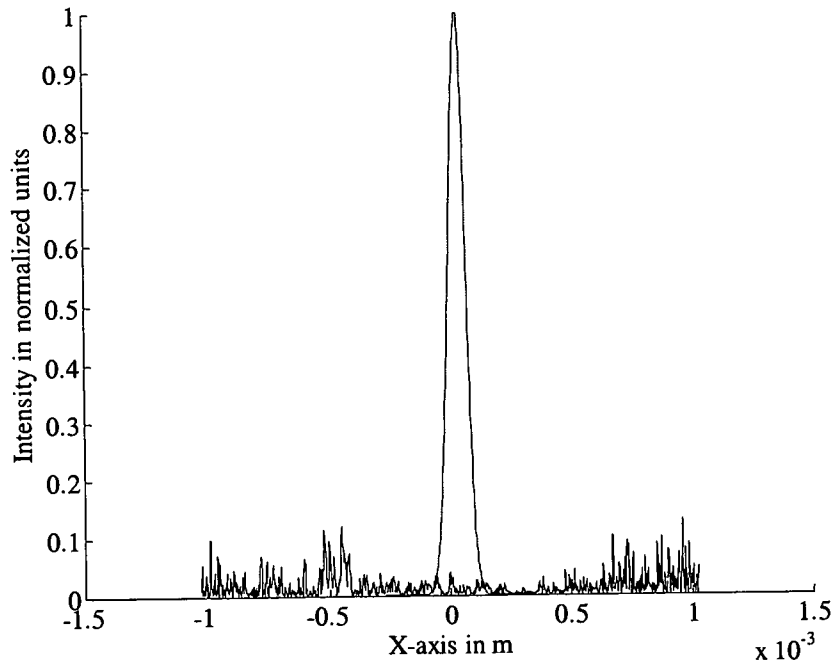


Figure 4.2b Backscattered beam (dotted) and original beam at the initial position for ten passes.

4.3 Simulation of Mutually Pumped Phase Conjugation in PR due to Two-Beam Mixing

To simulate mutually pumped phase conjugation in PR media using the theory presented in Sections 3.2 and 3.3, we investigate two-beam mixing between the contrapropagating beams. Accordingly, we allow two beams traveling in opposite directions to mix inside the crystal. The simulation is done for BaTiO₃ with the same set of parameters stated in Section 3.3. Simulation results are shown in Fig. 4.3 and Fig. 4.4. Although we have not seen phase conjugation in this case for the chosen set of

parameters, we intend to fully examine this case more rigorously to see if there is any phase conjugation.

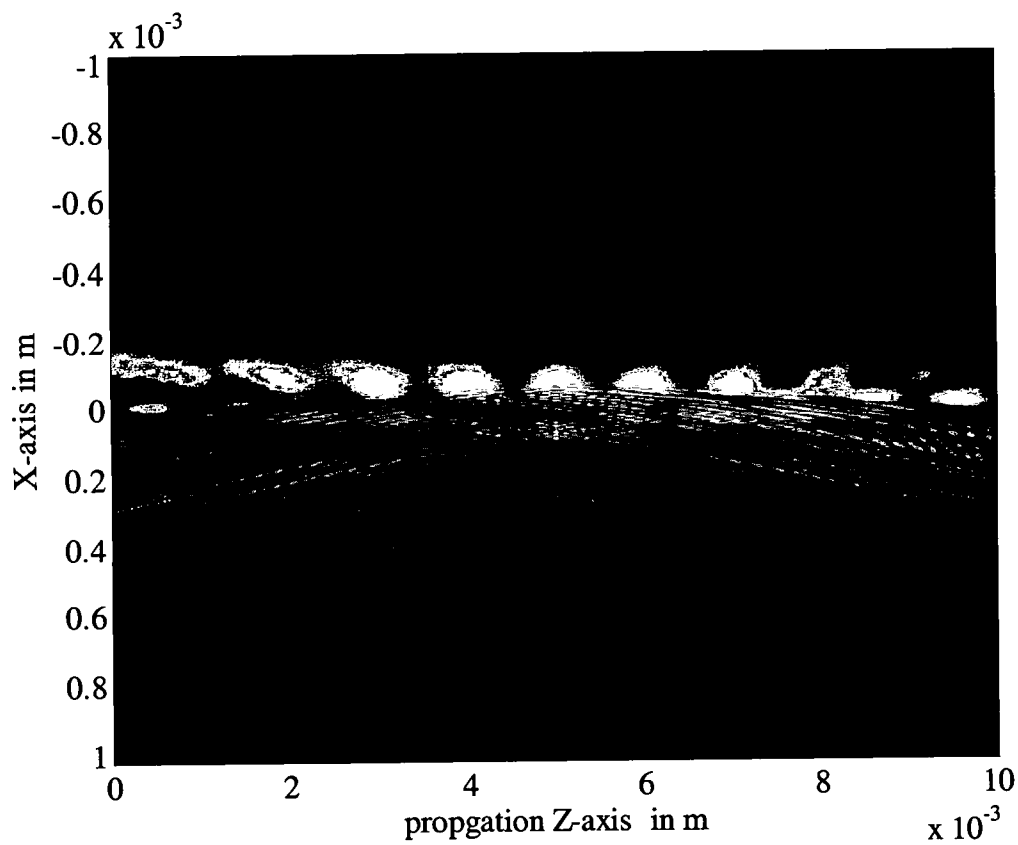


Figure 4.3 Contrapropagating beam mixing in PR media.

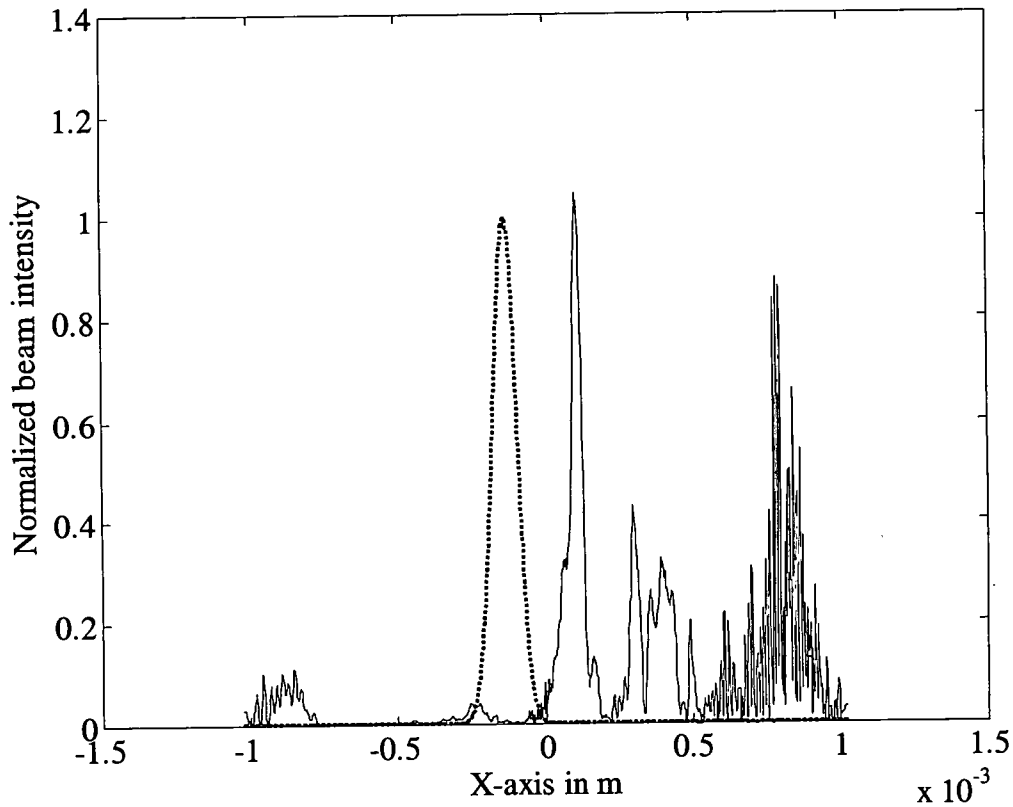


Figure 4.4 Backward traveling beam and original beam (dotted) at the initial position for one pass.

4.4 Summary, Conclusions and Future Work

In Chapter 1 we have presented an introduction to the theory of PR non-linear optics based on Kukhtarev equations and also the theory of grating formation and two-wave mixing in PR media. In Chapter 2 we have discussed the well know theory of beam propagation in nonlinear media using BPM and Fourier transforms. In Chapter 3 we presented the theory of induced refractive index in PR media. Using the theory and BPM technique stated in Chapter 2, we have simulated and analyzed DBF in diffusion

dominated PR crystals. Further by introducing the surface and bulk randomness in the media, we have studied the difference in DBF and RBF and also conditions at which one of them dominate over the other. These results have been tabulated in table3.1. Thereby, we have concluded that DBF is dominant for lower beam waists in order of tens of microns, the lower sample length and smaller inhomogeneities. As a logical extension to Chapter 3, we have tried to simulate phase conjugation effects in PR media. We infer from our simulation results that the occurrence of phase conjugation from backscattering cannot be substantiated from only back reflection from the crystal.

As future work we propose to

1. practically analyze the properties of DBF and RBF in diffusion dominated crystals using the conclusion presented Chapter 3;
2. look for phase conjugation results in other well known\ geometries edge reflection, four-wave mixing, etc.;
3. perform 2-D Gaussian beam analysis of DBF and RBF, which will be more precise than this work.

Appendix

Program I

Following is the Matlab code for Nonlinear Propagation in Kerr media

%Matalab code for Non linear Propagation Angular propagation of gaussian or sech
%beam in kerr type nonlinear medium and Fresnel transmission
%coefficients are added for each plane wave component done for TE case
% Arun Venkataraman

```
%
%  input data
%
close all;clear all;clc;
um=1e-6;
lambda = 1.55*um; % wavelength in microns
na=1; % refractive index of the indident medium generally air
nb = 3.5; % background(crystal) refractive index
n2 = 1.0e-16; % Kerr coefficient in cm^2/W
xmax = 300.0*um; % transverse domain size in microns
nx = 512; % number of transverse grid points
nz = 400; % number of z steps
Is = 1.0e13; % peak intensity in W/cm^2
x0 = 0.0; % soliton center displacement in microns
theta= 2; % incident angle in degrees
theta=theta*pi/180; %incident angle in radian
i=sqrt(-1);
N=1.8*1;
snell=(na/nb*theta)*180/pi
%
%  Set up of x-space variables and its K-space(K- X space) variables
%

kv = 2*pi/lambda; %K in vaccum
ka=kv*na; %K in medium one(air)
kb = kv*nb; %K in Medium(crystal)

dx = xmax/nx; %sampling period in X
```

```
kmax = 2*pi/dx;    %Maximum value of k (spatial freq domain)
dk = kmax/nx;      %step in Spatial freq
```

```
%Note:- nx is nothing but no. of FFT points its just a dimesionless
```

```
%
% Step of z-length and its spacing both in medium 1 & 2
%
```

```
ws = 1/(kv*sqrt(nb*n2*Is)) % soliton width for Is
I0 = N^2*Is                %initial intensity
zr=kb*ws^2/2                %rayleigh range
zmax=30*zr                  %Length of propagation
z1=3*zr                     %propagation distance in medium1 (linear medium)
z2=zmax-z1                  %propagation distance in medium1 (linear medium)
dz = zmax/nz;               %step size in propagation direction(z)
nz1=round(z1/dz);           %no. of step in medium 1
nz2=round(z2/dz);           %no. of steps in medium 2
```

```
%
% Set up of beam and linear phase
%
```

```
x=dx*(-nx/2 :nx/2-1);%space grid
s_1=[-nx/2 :nx/2-1];
kx=s_1*dk;%spatial frequency grid
kx=fftshift(kx);%is used shift the zero freq component to center which happens while
doing FFT
wave=2*sqrt(I0)./(exp((x-x0)/ws)+exp(-(x-x0)/ws));% sech beam
```

```
%
%linear propgation
%
```

```
eout = zeros(length(x),nz);
```

```
theta_a=theta+(kx/ka);
```

```

phasea=exp((-i)*kv*na*zmax*((theta_a).^2/2));
phase1=exp((-i)*kv*na*dz*((theta_a).^2/2));%phase in linear medium 1
% wave = fft(ifft(wave).*phasea);
for p = 1:nz1
    eout(:,p) = wave';
    wave = fft(ifft(wave).*phase1);
end

%
% end propagation
%

%check for angel
waven=abs(wave).^2;
xcenter1=x(waven==max(waven));

%
%adding angel of incidence and transmission coefficient to each plane wave component
%

theta_b=asin((na/nb)*sin(theta_a)) ;%using the snells law finding angel of refraction
T=2*sin(theta_b).*cos(theta_a)./sin(theta_a+theta_b);%calculating the transmission co-
efficient for each plane wave component
if theta==0, T(1)=T(2); end;

wave=ifft(T.*fft(wave));
phase2=exp((-i/2)*kv*nb*dz*((theta_b).^2/2));%phase in medium 2

figure(9);
plot(kx,(T),'.');

%
%
%

%Note:- all phase listed are same but for constant phase term which can
%be taken out as its going to remain constant but if you are trying to do
%phase analysis then make sure you add the exp(-i kv*nb*zmax) finally

%
% non -linear propagation
%
```



```

fig=round((nz-nz1)/3);

wavea(:,1)=wave';
art=1;
for p = nz1+1:nz
    wave = fft(ifft(wave).*phase2);
    wave = wave.*exp(i*dz*kv*n2*abs(wave).^2);
    wave = fft(ifft(wave).*phase2);
    eout(:,p) = wave';

    if p==nz1+art*fig
        wavea(:,art+1)=wave';
        art=art+1
    end
end
figure (10)
xlabel('x-axis in m')
ylabel('Beam intensity in W/cm^2');
for p= 1:4
    subplot(2,2,p);
    plot(x,abs(wavea(:,p)).^2);
    xlabel('x-axis in m')
    ylabel('Beam intensity in W/cm^2');
    title(['z =' p]);
end

%
%   End propagation
%

%check for the angel---- works only <= 1 order solitons

waven=abs(wave).^2;
xcenter=x(waven==max(waven));
angel=(xcenter-xcenter1)/z2*180/pi

```

```

%
%   Graphics
%

figure(3)
colormap(pink)
y=[0:zmax/nx:zmax];
imagesc(y,x,abs(eout).^2);

figure(4)
plot(x,abs(wave).^2);
animate(abs(eout).^2,x);

function [mov] = animate(arr,v)
if nargin < 2, v = [1:size(arr,1)]'; end
mx = max(max(arr));
mn = min(min(arr));
mnx = min(v);
mxx = max(v);
mov = moviein(size(arr,2));
for p = 1:size(arr,2)
    plot(v,arr(:,p));
    xlim([mnx,mxx]);
    ylim([mn,mx]);
    mov(:,p) = getframe;
end
end

```

Program II

Following is the MATLAB program for both DBF and RBF analysis.

```
%Deterministic and Random beam faning in Photorefractive Fe:BaTiO3(diffusion
dominated)
%Feb 22 2006
%Arun Venkataraman

%
%  input data
%

close all;clc; clear all;
um=1e-6;mm=1e-3;cm=1e-2;

lambda = .514*um;    % wavelength in microns
na=1.0;               % refractive index of the incident medium generally air
nc=1.0;               % refractive index of the medium3 generally air

nx =1024*2^3;         % number of transverse grid points
nz = 400;             % number of z steps

ws=100*um;           %waist b4 crystal surface if z1=1*zr
w0=ws/sqrt(2);        %intial waist
dx=2*um;              %sampling length in x axis
nos=ws/dx             %no. of sample points at the waist while entering the crystal
xmax=dx*nx;           %transverse domain

p=1.6e-3;             % peak intensity in W/m^2
Is = p/w0^2;
x0 = 0;               % displacement from center in microns
theta=0;              % incident angle in degrees
theta=theta*pi/180;
nu=55;                %angel between the c-axis and the x-axis(incident plane)
nu=nu*pi/180;
i=sqrt(-1);
N=1;

Kb=1.3806503e-23;     %boltzmann const
t=300;                %Temperature
e=1.60217646e-19 ;    %Elementry charge
beta=2;               %in s-1
s=2.6e-5;
```

```

eta=377;           %characterstic impedance
r42=1640e-12;      %generally in pm/V
r13=8e-12;
r33=28e-12;

n0=2.488;
ne=2.434;
nb =(n0+ne)/2

%
%   Set up of x-space variables and its K-space(K- X space) variables
%

kv = 2*pi/lambda;   %K in vaccum
ka=kv*na;           %K in medium one(air)
kb = kv*nb;         %K in Medium(crystal)
kc=kv*nc;           %K in medium three(air)
kmax = 2*pi/dx;     %Maxium value of k (spatial freq domain)
dk = kmax/nx;       %step in Spatial freq domain

%Note:- nx is nothing but no. of FFT points its just a dimensionless

%
%   Step of z-length and its spacing both in medium 1 & 2
%

I0 = N^2*Is;        %initial intensity
zr=kv*w0^2/2        %Raleigh range
z1=1*zr;
z2=.5*cm             %propagation distance in crystal
z3=10*zr;
zmax=z2              %Length of propagation
dz = zmax/nz;        %step size in propagtion direction(z)
nz2=round(z2/dz);    %no. of steps in medium 2

%
%   Set up of beam and linear phase
%
```

```

x=dx*(-nx/2 :nx/2-1);           %space grid
s_1=[-nx/2 :nx/2-1];
kx=s_1*dk;                       %spatial frequency grid
kx=fftshift(kx);                 %is used shift the zero freq component to center which happens
while doing FFT

```

```

% wave=2*sqrt(I0*eta)./(exp((x-x0)/w0)+exp(-(x-x0)/w0)); % sech beam

```

```

wave=2*sqrt(I0*eta)./exp((x-x0).^2/w0^2); %Gaussian Beam

```

```

%
%linear propgation
%

```

```

%Note:- all phase listed are same but for constant phase term which can
%is taken out as it's going to remain constant but if you are trying to do
%phase analysis then make sure you add the exp(-i kv*nb*zmax) finally

```

```

theta_a=theta+(kx/ka);
phase1=exp(-i*kv*na*z1*sqrt(1-theta_a.^2)).*exp(i*kv*na*z1); %non paraxial phase
wave = fft(ifft(wave).*phase1);

```

```

%
%adding angel of incidence and transmission coefficients to each plane wave
%component
%

```

```

theta_b=asin((na/nb)*sin(theta_a)) ; %using the snells law finding angel of refraction

```

```

T=2*na*cos(theta_a)./(na*cos(theta_a) + nb*cos(theta_b));           %calculating the
transmission co-efficient for each plane wave component
if theta==0, T(1)=T(2); end;

```

```

wave=fft(T.*ifft(wave));

```

```

% wave=fft(T.*ifft(wave)).*(1.0+(rand(size(x))-0.5)*.1).*exp(i*.1*(rand(size(x))-
0.5)); %Random beam fanning due surface randomness

```

```

%
%    non -linear propagation
%

nu=theta_b+nu;
fnu=-0.5*nb.^3.*cos(nu).*(r13*sin(nu)+2*r42*sin(nu).^2+r33*cos(nu).^2);
phase2=exp(-(i/2)*kv*nb*dz*sqrt(1-theta_b.^2)).*exp(i/2*kv*nb*dz);%Phase in medium
2 non- paraaxial

```

```

for p = 1:nz2
    eout(:,p) = wave';
    %    wave = fft(ifft(wave).*phase2);
    wave = fft(ifft(wave).*phase2).*(1.0+(rand(size(x))-
0.5)*01/nz2).*exp(i*01/nz2*(rand(size(x))-0.5));%random beam fanning due to bluk
random
    dI=diff(abs(wave).^2);
    dI=([dI dI(max(size(dI)))])/dx;
    Esc=(Kb*t/e).*(dI/(eta*beta/s+abs(wave).^2));
    deln=fft(ifft(Esc).*fnu);
    wave = wave.*exp(-i*dz*kv*deln);
    wave = fft(ifft(wave).*phase2 );

end

```

```

figure(4);%Image inside the crystal
colormap(pink)
y=[0:z2/nz2:z2];
imagesc(y,x,abs(eout).^2);

```

```

theta_c=asin(na/nc*sin(theta_b)) ;    %using the snells law finding angel of refraction

```

```

T2=2*sin(theta_b).*cos(theta_a)./(sin(theta_b+theta_c).*cos(theta_b-
theta_c));%calculating the transmission co-efficient for each plane wave component
if theta==0, T2(1)=T2(2); end;
wave=fft(T2.*ifft(wave));
figure(15);
plot(x,abs(wave).^2,'b');

```

```

phase3=exp(-i*kv*na*z3*sqrt(1-theta_b.^2)).*exp(i*kv*na*z3);%Phase in medium 2
non- paraxial
wave=fft(ifft(wave).*phase3);

```

```

figure(11);%Just Farfield will have more noise for deterministic beam fanning
% hold on
plot(x,abs(wave).^2/max(abs(wave).^2));
waveout=wave;
ylabel('Normalized beam intensity')
xlabel('X-axis in m');

```

References

- [1] P.P. Banerjee and R. Misra, "Dependence of photorefractive beam fanning on beam parameters", *Opt. Comm.* **100** 166-172 (1993).
- [2] J.J. Liu, P.P. Banerjee and Q. Song, "Role of diffusive, photovoltaic, and thermal effects in beam fanning in LiNbO_3 ", *J. Opt. Soc. Amer. B* **11** 1688-1693 (1994).
- [3] C. Mailhan, M. Goetz, N. Fressengeas and G. Kugel, "Insight into a new geometrical approach to beam fanning in BaTiO_3 ", *J. Opt. Soc. Amer. B* **18** 64-74 (2001).
- [4] S. Solanki, X. Xu and T.C Chong, "DBF in Fe-doped stoichiometric lithium niobate crystals, *Appl*", *Opt.* **44** 4922-4929 (2005).
- [5] A. Ashkin, G.D. Boyd, J.M. Dziedzic, R.G. Smith, A.A. Ballman, J.J. Levinstein and K. Nassau, "Optically induced refractive index inhomogeneities in LiNbO_3 and LiTaO_3 ", *Appl. Phys. Lett.* **9** 72-74 (1966).
- [6] P. Gunter and J. P. Huignard, *Photorefractive Materials and Their Applications, I and II*. New York: Springer-Verlag, 1987.
- [7] V.L. Vinetskii, N.V. Kukhtarev, S.G. Odulov and M.S. Soskin, "Dynamic self-diffraction of coherent light beams", *Sov. Phys-Usp.* **22** 742-756 (1979).
- [8] N.V. Kukhtarev, V.B. Markov, S.G. Odulov, M.S. Soskin and V.L. Vinetskii, "Holographic storage in electro-optic crystals, beam coupling and light amplification", *Ferroelectrics* **22** 961-964 (1979).

- [9] N.V. Kukhtarev, "Kinetics of hologram recording and erasure in electrooptic crystals", Soc. Tech. Phys. Lett. **2** 438–440 (1977).
- [10] N.V. Kukhtarev, V.B. Markov, S.G. Odoulov, M.S. Soskin and V.L. Vinetskii, "Holographic storage in electrooptic crystals", Ferroelectrics **22** 949–964 (1979).
- [11] P. Yeh, "Two-wave mixing in nonlinear media", IEEE J. Quantum Electron. **25** 484–519 (1989).
- [12] P. Yeh, "Fundamental limit of the speed of photorefractive effect and its impact on device applications and material research", Appl. Opt. **26** 602–605 (1987).
- [13] P. Banerjee, *Nonlinear optics: Theory, Numerical modeling and Applications*, Marcel Dekker, Inc , New York 2004.
- [14] T.C. Poon and P.P. Banerjee, *Contemporary optical image processing with MATLAB*, Elsevier, Oxford 2001.
- [15] D. Gabor, "Associative holographic memories", IBM J. Res. Dev. **13** 156–159 (1969).
- [16] J. Khoury, J.S. Kane, G. Asimellis, M. Cronin-Golomb and C. Woods, "All-optical nonlinear joint Fourier transform correlator", Appl. Opt. **33** 8216 (1994).
- [17] M.A. Neifeld and D. Psaltis, "Programmable image associative memory using an optical disk and a photorefractive crystal", Appl. Opt. **32** 4398–4409 (1993).
- [18] F.T.S. Yu, S. Yin and C.M. Bang, "A content-addressable polychromatic neural net using a specially doped LiNbO₃ photorefractive crystal", Opt. Comm. **107** 300 (1994).
- [19] C. Denz, *Optical Neural Networks*, FIZ Karlsruhe, Germany: Vieweg: Braunschweig, 1999.

- [20] A. Marrakchi, W.M. Hubbard, S.F. Habiby and J. S. Patel, "Dynamic holographic interconnects with analog weights in photorefractive crystals", *Opt. Eng.* **29** 215-224 (1990).
- [21] J. Hong, A.E. Chiou and P. Yeh, "Image amplification by two-wave mixing in photorefractive crystals", *Appl. Opt.* **39** 3026-3029 (1990).
- [22] K. Sayano, G.A. Rakuljic and A.Yariv, "Thresholding semilinear phase conjugate mirror", *Opt. Lett.* **13** 143-145 (1988).
- [23] J. Joseph, K. Kamra, K. Singh, and P.K.C Pillai, "Real-time image processing using selective erasure in photorefractive two-wave mixing", *Appl. Opt.* **31** 4769-4772 (1992).
- [24] Y. Uesu, S. Kurimura, T. Aoyama and E. Kubota, "Recent development of optical novelty filter and dynamics of optical novelty filter with use of the CAT-type self-pumped phase conjugate mirror", *Ferroelectrics* **174** 133-148 (1995).
- [25] J.H. Hong and T.Y. Chang, "Frequency-agile rf notch filter that uses photorefractive two-beam coupling", *Opt. Lett.* **18** 164-166 (1993).
- [26] J. Khoury, V. Ryan and M. Cronin-Golomb, "Photorefractive frequency converter and phase-sensitive detector", *J. Opt. Soc. Am. B* **10** 72-82 (1993).
- [27] R. Scarmozzino, A. Gopinath, R. Pregla and S. Helfert, "Numerical Techniques for Modeling Guided-Wave Photonic Devices", *IEEE J. Quantum Electron.* **6** 150-162 (2000).
- [28] Van Roey, J. van der Donk and P.E. Lagasse, "Beam-propagation method: analysis and assessment", *J. Opt.Soc. Am.* **71** 803 (1981).
- [29] D. Yevick and L. Thylen, "Beam Propagation Method Analysis of Gratings", *J. Opt. Soc. Am.* **72** 1084 (1982).

R002592749

- [30] R. Baets and P. E. Lagasse, "Calculation of radiation loss in integrated-optic tapers and Y-junctions", *Appl. Opt.* **21** 1972 (1982).
- [31] C. R. Pollock, *Fundamentals of Optoelectronics*, Irwin, New York, 1995.
- [32] M.D. Feit and J.A. Fleck, "Light propagation in graded-index optical fibers," *Appl. Opt.*, **17** 3990–3998 (1978).
- [33] D. Yevick, "A guide to electric field propagation techniques for guided-wave optics", *Opt. Quantum Electron.* **26** 185–197 (1994).
- [34] J. Feinberg, "Self-pumped, continuous-wave phase conjugator using internal reflection", *Opt. Lett.* **7** 486-488 (1982).
- [35] M. Segev, Y. Ophir and B. Fischer, "Nonlinear multi two-wave mixing, the fanning process and its bleaching in photorefractive media", *Optics Communications* **77** 265-274 (1990).